SANDIA REPORT

SAND98–2043
Unlimited Release
Printed September 1998

A Combustion Model for the TWA 800 Center-Wing Fuel Tank Explosion

Melvin R. Baer and Robert J. Gross

Prepared by
Sandia National Laboratories
Albuquerque, New Mexico 87185 and Livermore, California 94550

Sandia is a multiprogram laboratory operated by Sandia Corporation, a Lockheed Martin Company, for the United States Department of Energy under Contract DE-AC04-94AL85000.

Sandia National Laboratories

Issued by Sandia National Laboratories, operated for the United States Department of Energy by Sandia Corporation.

Available to DOE and DOE contractors from
Office of Scientific and Technical Information
P.O. Box 62
Oak Ridge, TN 37831

Prices available from (615) 576-8401, FTS 626-8401

Available to the public from
National Technical Information Service
U.S. Department of Commerce
5285 Port Royal Rd
Springfield, VA 22161

NTIS price codes
Printed copy: A03
Microfiche copy: A01

DISCLAIMER

Portions of this document may be illegible in electronic image products. Images are produced from the best available original document.

SAND98-2043
Unlimited Release
Printed September 1998

A Combustion Model For The TWA 800 Center-Wing Fuel Tank Explosion

Melvin R. Baer and Robert J. Gross
Energetic and Multiphase Processes Department
Sandia National Laboratories
P. O. Box 5800
Albuquerque, New Mexico USA 87185-0834

Abstract

In support of the National Transportation Safety Board investigation of the TWA Flight 800 accident, a combined experimental/computational effort was conducted that focused on quarter-scale testing and simulation of the fuel-air explosion in the Boeing 747 center wing fuel tank. This report summarizes the modeling approach used at Sandia National Laboratories. In this approach approximations are introduced that capture the essential physics associated with turbulent flame propagation in multiple compartment fuel tanks. This model efficiently defines the pressure loading conditions during a jet-fuel air explosion in a fuel tank confinement. Modeling calculations compare favorably with a variety of experimental quarter-scale tests conducted in rigid confinement. The modeling describes well the overpressure history in several geometry configurations. Upon demonstrating a reasonable comparison to experimental observations, a parametric study of eight possible ignition sources is then discussed. Model calculations demonstrate that different loading conditions arise as the location of the ignition event is varied. By comparing the inferred damage and calculated impulses to that seen in the recovered tank, it may be possible to reduce the number of likely sources. A possible extension of this work to better define tank damage includes coupling the combustion model as a pressure loading routine for structural failure analysis.

This work was supported by the United States Department of Energy under Contract DE-AC04-94AL85000. Sandia is a multiprogram laboratory operated by Sandia Corporation for the United States Department of Energy.

Table of Contents

List of Figures

1.0 Introduction

As part of the investigation of the TWA Flight 800 accident, the National Transportation Safety Board (NTSB) sponsored a combined experimental and modeling study associated with a fuel-air explosion in the Boeing 747-100 center wing tank (CWT) [1]. The purpose of this study is to identify the nature and cause of ignition and propagation of a Jet A fuel-air explosion that most likely occurred in the heated fuel tank[1]. Ultimately, the source of ignition can be potentially identified by determining a most probable ignition location within the multiple compartment fuel tank. In assessing the origin and nature of the explosion, accelerated combustion behavior of the explosion has to be unraveled consistent with the observed damage in the recovered CWT. In these reverse calculations, a combustion model provides pressure histories in the various compartments of the CWT. Potential sources of ignition can then be linked to the location where the combustion began by evaluating the resulting damage based on structural failure analysis. Hopefully, the pressure histories provide a unique loading condition for this determination.

To model the pressure loading for structural failure, it is necessary to describe the reactive fluid dynamics of the explosion. Flame propagation involves a complex interaction of physical and chemical processes and a detailed first principles calculation of transient turbulent reactive flow is beyond current computational capabilities, even with the state-of-the-art massively parallel computers. Current descriptions use submodels that effectively describe the essential physical phenomena of the reactive flow. To achieve a reasonable level of predictability, modeling must be coupled to laboratory and scaled test measurements.

In this work, quarter-scale experiments were conducted by researchers at the California Institute of Technology [2] using the site facilities, instrumentation and support of the Applied Research Associates [3] in Denver, Colorado. Computational and experimental efforts for this study are complementary in several ways. For example, the submodels necessary to make the computations tractable rely on experiment measurements to provide several key parameters such as the turbulent flame velocities and heat transfer effects. Confidence in the combustion model is gained by applying the model to a variety of experiments. Experimental tests are typically time-consuming and expensive. Once benchmark experiments calibrate the computational model, the model can then be used to investigate a wider variation of effects including geometry, ignition location, *etc.* On the basis of scaled testing, modeling can also investigate a variety of initial conditions for the full-scale CWT geometry that may be very difficult to experimentally replicate.

---

1. The NTSB and Boeing conducted a series of flight tests using a specially instrumented Boeing 747-100 retracing the flight path conditions of TWA 800. Temperature and gas sampling measurements in the CWT showed that the fuel tank ullage was heated to temperatures in excess of 120F prior to takeoff with a slight temperature drop at the leveling attitude of 19,000 ft., consistent with the time of the incident. At these conditions, the fuel-air mixture readily ignites by low energy sources. Details of these tests can be found in Reference [4].

Since time constraints for analysis in this study required using existing modeling capabilities, with minimal modifications, the combustion modeling developed by Sandia National Laboratories follows an approach used in assessing hydrogen combustion in nuclear reactor vessels [5]. This modeling easily adapts to parametric and sensitivity analysis. Extensions of this prior work included incorporating a three-dimensional flame propagation routine for multiply-connected regions with Jet-A fuel-air thermochemistry. This modeling is largely based on prior experimental studies which were successfully used in hazards analysis. Prior work has suggested that the salient features of the pressurization can be determined, provided that certain approximations remain valid. These assumptions lead to a description that is readily amenable for computation and retains the strong interaction of chemical energy release and the dynamics of fluid motion. Furthermore, this approach easily adapts to structural analysis as a forcing routine. To completely determine the response of a dynamically-failing CWT, including venting effects to a cargo hull or ambient environment, the coupling of the failure of the tank structure during flame propagation is ultimately necessary.

In the following sections, a model for flame propagation in a multiple compartment enclosure is described. This modeling is based on conservation equations approximated for the limit of small Mach number flow (flame speed/sound speed) [6]. At these conditions, the mean pressure is spatially uniform within each individual compartment. However, a pressure gradient across the whole enclosure of the CWT takes place due to the presence of flow restrictions connecting compartments.

In approximating the combustion, a thin flame assumption is used, *i.e.* the flame is treated as a density and entropy discontinuity that is propagated at a prescribed velocity consistent with localized flow conditions. Flame propagation is constructed by intersecting spherical segments that expand from multiple ignition locations. For example, as the flame spreads over the enclosure walls, individual flames spawn and propagate at flow passages to connecting compartments and a complex flame surface evolves with time. A three-dimensional adaptive interface tracker is described that accurately determines the burn gas volume and surface area in each compartment. Since gas motion is induced ahead of the flame, gas motion within each compartment takes place that is restricted by "orifices" connecting the compartments. The resulting flow at these locations induces localized jets that stir the unburned gases in the compartments, producing turbulence to enhance the rate of combustion. Empirical correlations based on existing literature data are used to specify the turbulent flame velocity of the gas mixture.

Consistent with the flame sheet approximation, the change in gas density, temperature, and composition are estimated from equilibrium thermodynamic calculations using routines in CHEMKIN [7]. Radiation and convective heat transfer in the burned and unburned regions are also included. For the radiation heat transfer, absorption and emission coefficients are determined using an exponential wide-band model [8] (based on the gas species present) and a heat transfer coefficient for the turbulent convective flow is estimated from the post combustion decay rate of the pressure.

In the sections to follow, details of the combustion model and associated fluid dynamics are first described. Then, the numerical adaptive flame propagation algorithm is outlined. Model formulations for the thermochemistry and turbulent flame velocity are also given. The CalTech laboratory tests (HYJET) [9] are used as a preliminary assessment of the model. Based on a determination of combustion parameters, the model is then applied to a variety of tests conducted in one-quarter scale experiments of the CWT. These experiments used a single test apparatus with removable walls whereby the number of compartments is modified by excluding various panels. Additionally, the facility incorporates multiple ignition sources so that the location of ignition can also be varied. To reproduce the combustion behavior of the light components of Jet A aircraft fuel with low pressure air, tests were conducted using a mixture of propane and hydrogen[1] as the combustion gas to simulate the Jet A fuel used in commercial aircraft [10].

Since structural failure analysis is not included in the current work, the walls of the compartments are assumed to be rigid, *i.e.* the pressure difference between compartments does not cause strain or displacement that subsequently leads to pressure relief due to venting. Hence, pressure differences and delivered impulse between compartments are overestimated. Roughly, fourteen tests in the rigid configuration are described and modeled. Based on a preliminary assessment, a parametric study of the pressure loading due to varying the ignition location was performed and demonstrates that the pressure loadings are different and dependent on the ignition origin. This establishes that an inverse structural failure analysis may provide a means for determining the source of the ignition event.

1. Tests at the CalTech facilities demonstrate that a mixture of hydrogen and propane with low pressure air can effectively replicate the turbulent flame propagation behavior of the light distillate components of Jet A. Similar overpressure and burn velocities are observed. This greatly simplified experimental tests by avoiding the necessity of heating liquid Jet A fuel and provided a well-defined means for controlling the composition of the fuel air mixture.

2.0 Mass and Energy Conservation

The complete thermal/chemical/mechanical processes that occur during flame propagation in an enclosed vessel includes the effects of mass, momentum and energy transport, turbulence, heat transfer due to convection and thermal radiation, chemistry, acoustics, and structural mechanics (*i.e.* displacement and damage of structural confinement leading to venting effects). Each one of these processes have different resolution requirements with a large disparity of length and time scales. Solving all of the details in a system of field equations, from first principles, is beyond the capacity of even the fastest computers. Furthermore, the problem of interest has to consider three-dimensional combustion in a multiply-connected structure with complex geometry. Even with the use of simplified geometry and approximations to reduce the complexities of the field equations, describing the classical combustion problem of a propagating turbulent flame sheet in an enclosure requires the use of submodels for phenomena that cannot be highly resolved. The approach used in this work is based on key assumptions that reduce the model to a description requiring only a few minutes of computational time on a workstation.

To simplify the fluid dynamics associated with the explosion, an approximation is introduced which neglects the effects of acoustic waves. This leads to a description that is much easier to resolve numerically. This approximation remains valid if the flow velocity is much less than the speed of sound. With this approximation the flow equations reduce to solving only the mass and energy conservation equations constrained by the condition that the gas pressure changes only with time, or $P(\mathrm{x,y,z,t}) \Rightarrow P(\mathrm{t})$. Thus, as the flame moves through the entire volume, each compartment becomes uniformly pressurized. The pressure varies from compartment to compartment due to flow restrictions connecting the compartments.

As an additional assumption, the combustion is treated as a moving interface separating burned and unburned gases. The expanding burned gases induce flow ahead of the flame front and burned gases are pushed away in an opposite direction from the flame front. Thus, a mean flow induces turbulence, and as the flame moves into unburned material its surface becomes wrinkled, accelerating the rate of propagation. Resolving all of these details of the complex combustion behavior is an exceedingly difficult modeling task [11]. An alternative approach describing these effects uses empirical corrections of the flame velocity based on experimental observations. The experimental turbulent flame propagation studies of Bradley and his colleagues [12] are used to describe the effects of accelerated combustion.

The properties of the burned gases are estimated using ideal gas thermochemical equilibrium calculations. Since the pressure of the unburned gases varies, many equilibrium states are expected and the method for computing the burned gas temperature and composition is based on assuming that the pressure is continuous across the flame; this is a valid assumption as long as the flame is subsonic (in keeping with the low-speed flow requirement).

Since the pressures within the compartments determine the loading of the tank structure, the equations of motion are simplified by replacing the differential field equations with volume-mean quantities based

on formal mathematical manipulation. The final description reduces to a set of coupled ordinary differential equations that are a function only of time. This description is easily solved using standard numerical methods. Coupled to this set of integral equations is a flame propagation adaptive routine with an empirical burn law to determine the mean flame volume and surface area. A chemical equilibrium solver is used to define the properties of the burned gases. The coupling of the flow between compartments is represented using well-known "orifice" flow relationships based on pressure differences between connected regions. Since these flow restrictions produce localized turbulent flows leading to flame acceleration, turbulence properties of the mean flow in individual compartments are estimated based on similarity characteristics of turbulent jets. The effects of energy loss and subsequent loss of pressure due to convective and radiative heat transfer are included using well-accepted models requiring input of the composition and temperature of the reacted gases determined by the chemical equilibrium routine.

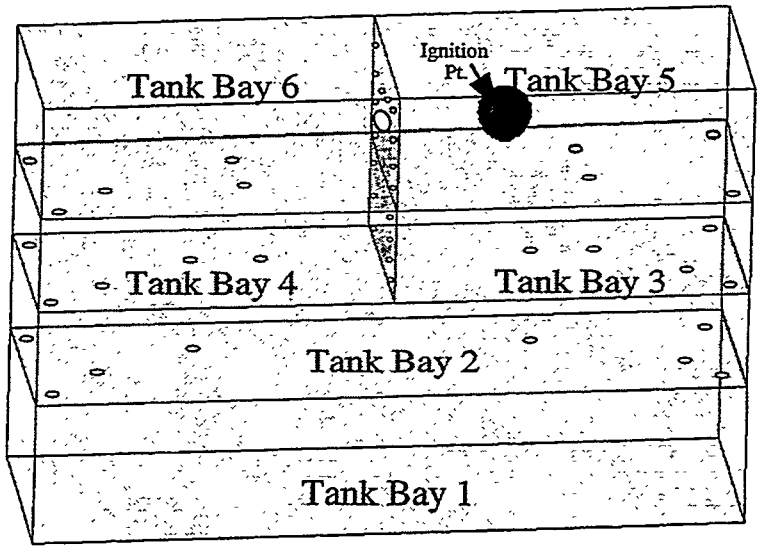

Figure 1. Typical six compartment test configuration. Circles in the walls represent flow passages between compartments.

Based on the above assumptions, the CWT is represented as a control volume connecting a group of compartments as displayed in Figure 1. The compartments are assumed to be rectangular in shape and are connected by an arbitrary number flow orifices that allow flow communication between compartments and also serve as ignition centers of flame propagation in adjoining compartments. The burned and unburned volumes are separated by thin flame fronts separating low- and high-temperature regions assumed to be composed of ideal gases:

$$P = \rho RT, \tag{1}$$

where ρ is density, R is the gas constant, T is temperature, P is the pressure. The volume, V, although not used explicitly in Equation (1), can be associated with the equation of state and is introduced here.

In approximating the flame to represent a jump state in density and entropy, a more useful form of the ideal gas equation is given as:

$$P = k\rho^{\gamma}e^{\phi} \tag{2}$$

where k is a constant, γ is the isentropic index, and $\phi = s/C_v$ where s is entropy and C_v is the specific heat at constant volume. ϕ is termed the normalized entropy. Equation (2) is then given as:

$$\ln\rho = \frac{1}{\gamma}\ln P - \frac{\phi}{\gamma} + \tilde{k} \tag{3}$$

where $\tilde{k}$ is also a constant.

An application of the chain rule for density variations as a function of pressure and normalized entropy is given as:

$$\frac{1}{\rho}\frac{d\rho}{dt} = \left(\frac{1}{\rho}\frac{\partial\rho}{\partial p}\right)\frac{dp}{dt} + \left(\frac{1}{\rho}\frac{\partial\rho}{\partial\phi}\right)\frac{d\phi}{dt} \tag{4}$$

In the above relationship it is also assumed that in the unburned and burned regions the entropy is spatially invariant and only varies across the flame surface. Conservation of mass states:

$$\frac{1}{\rho}\left(\frac{\partial\rho}{\partial t} + \hat{v}\cdot\nabla\rho\right) = \frac{1}{\rho}\frac{d\rho}{dt} = -\nabla\bullet\hat{v} \tag{5}$$

where $\hat{v}$ is the gas velocity vector. By combining Equations (4) and (5), the following is obtained:

$$-\nabla\bullet\hat{v} = \frac{1}{\gamma p}\frac{dp}{dt} - \frac{1}{\gamma}\frac{d\phi}{dt} \tag{6}$$

Gauss' s Theorem is applied for analysis of the compartment volume effects; the Theorem relates surface transport to the volumetric changes and is given by::

$$\int_{Vol} \nabla\bullet\hat{v}\,dV = \oint_{Surface} \hat{v}\bullet dA \tag{7}$$

This theorem is applied separately to the burned and unburned region within each compartment. Since the right-hand side of Equation (6) contains a material derivative, integrating over the burn and unburned volumes includes effects of flow into and out of the control volumes. This results in expressions for the normal velocities as:

$$v_b \cdot A_f = -\frac{V_b}{\gamma_b}\left\{\frac{1}{p}\frac{dp}{dt} - \frac{d\phi_b}{dt}\right\} - \int_{S_b} \hat{v} \bullet dA \tag{8}$$

$$v_u \cdot A_f = -\frac{V_u}{\gamma_u}\left\{\frac{1}{p}\frac{dp}{dt} - \frac{d\phi_u}{dt}\right\} - \int_{S_u} \hat{v} \bullet dA \tag{9}$$

where the subscript "b" refers to the burned region and the subscript "u" refers to the unburned region, A_f is the mean area of the flame and the integrals in Equations (8) and (9) account for flow in or out of each region.

To include the effects of heat loss (or gain) in each region (symbol $\hat{q}$) the energy conservation equation, in terms of entropy, is given in the form:

$$\rho T\frac{ds}{dt} = \nabla \bullet \hat{q} \tag{10}$$

Integrating Equation 10 over the burned and unburned regions yields leading order effects of heat transfer in terms of normalized entropy:

$$\frac{d\phi_b}{dt} = \frac{(\gamma_b - 1)Q_b}{pV_b} \tag{11}$$

and

$$\frac{d\phi_u}{dt} = \frac{(\gamma_u - 1)Q_u}{pV_u} \tag{12}$$

where Q_b and Q_u represent heat loss or gain from the burned and unburned region, respectively, and, V_b and V_u are the volumes of the burned and unburned regions. A positive value of Q implies an energy gain wheras a negative value corresponds to heat loss.

By definition, the burn velocity, μ, is introduced that includes the effects of turbulence:

$$v_u - v_b = \mu(E-1) \tag{13}$$

where $E = \rho_u/\rho_b$ is the expansion ratio across the flame discontinuity. Thus, the conservation of mass across the flame discontinuity relates the burn velocity to the observed flame velocity, $\mathcal{V}_f$:

$$E(v_u - \mathcal{V}_f) = (v_b - \mathcal{V}_f) \tag{14}$$

By combining Equations (8), (9), (11), (12), and (13) the pressure within an individual compartment is defined as:

$$\frac{1}{p}\frac{dp}{dt} = \frac{\mu(E-1)A_f + [\text{Orifice Terms}] + \dfrac{V_u}{\gamma_u}\dfrac{d\phi_u}{dt} + \dfrac{V_b}{\gamma_b}\dfrac{d\phi_b}{dt}}{\left\{\dfrac{V_u}{\gamma_u} + \dfrac{V_b}{\gamma_b}\right\}} \tag{15}$$

where the orifice terms account for flow in or out of the connected compartments. Equations (11), (12), and (15) form three coupled ordinary differential equations with the unknowns p, pressure, ϕ_u, the unburned normalized entropy, and ϕ_b, the burned normalized entropy for a single compartment. Thus, the total number of equations for the total region of connected compartments equals three times the number of compartments. Note that for each compartment $V_u = V_{\text{total}} - V_b$.

Orifices fall into separate classes depending on whether the gas flow is venting burned or unburned gases. The flow in or out of each region depends on the relative pressures of the connected compartments. Thus, in keeping with an "orifice" flow model, the flow corrections to Equation (15) are:

$$[\text{Orifice Terms}] = [v_b A_{\text{burn inlet}} - v_b A_{\text{burn outlet}} + v_u A_{\text{burned inlet}} - v_u A_{\text{unburned outlet}}]. \tag{16}$$

Closure of the system of equations is obtained by determining and/or specifying the variables $\mu, E, A_f, V_u, V_b, \gamma_u, \gamma_b, Q_u$, and Q_b.

3.0 Thermochemical Equilibrium Analysis

The properties of the unburned and burned gases, such as temperature and composition, are obtained from thermochemical equilibrium calculations. The equilibrium routines from CHEMKIN [7] are used in this work. Since numerous state evaluations are expected, a selected set of combustion products are considered in the thermochemical library. Typically, for Jet A/air or propane/hydrogen/air mixtures, the species of most importance include Jet A fuel, C_3H_8, O_2, N_2, Ar, CO_2, H_2O, H_2, CO, NO, OH, H, O, C and C(s). Propane is included in this species set because a mixture of hydrogen and propane is used as a simulant for the light components of Jet A fuel. Argon is included as a minor constituent of air. The species carbon dioxide, water vapor and carbon monoxide are the well-known "greenhouse" gases that contribute to thermal radiation effects. The radical hydroxide, hydrogen and oxygen species are included for dissociation effects at high temperatures. Similarly, the condensed phase carbon is included for fuel-rich mixtures from which one expects the formation of soot.

With this reduced set of species, thermochemical calculations for constant volume or pressure states are efficiently evaluated. As the flame propagates, the jump in thermodynamics states for a deflagration is represented by a constant pressure calculation and the final overpressure in a confined volume (excluding heat loss) is estimated using isochoric (constant volume) state analysis. Figure 2 compares the CHEMKIN calculational equilibrium isochoric overpressure versus. fuel/air mass ratio to experimental measurements for Jet A/air mixtures initially at 0.585 atm. and 373 K. As expected, the calculations predicts higher overpressures than observed, particularly for lean fuel-air mixtures. These differences are due to heat loss nonequilibrium effects that are not included in equilibrium analysis. These equilibrium calculations correspond identically to those reported in Reference [10], which provides a consistency check for the modeling.

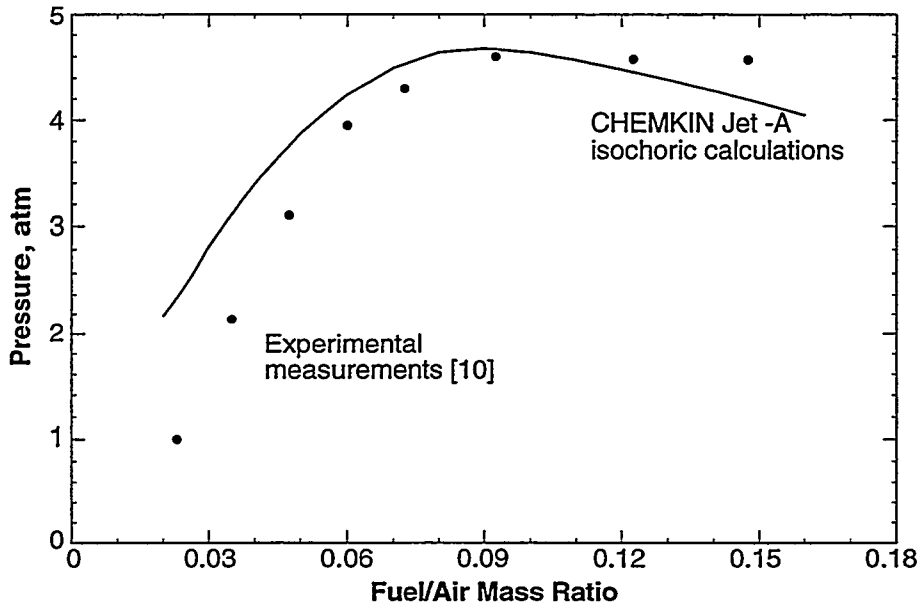

Figure 2. Comparison of calculated adiabatic constant volume overpressures to experimental results for Jet A at 0.585 atm and 373 K.

4.0 Flame Surface Area and Volume

In determining the overpressure and the heat loss during the propagation of the flame in the CWT, the flame surface area, A_f, and the unburned and burned volumes, V_b and V_u, are required as a function of time. These quantities are defined based on an algorithm that first determines if a region contains a segment of a flame interface. If the region contains an interface, a subgrid structure is embedded to encompass it and resolves the area and volume. Most importantly, this algorithm uses unstructured mesh information and integer logic for interface tracking. Figure 3 depicts a rectangular three-dimensional region that has several flame sheets moving into it at time, t. A fixed origin of the system is defined and a set of ignition locations are specified. Then a collection of spherically growing flames expand from the ignition locations at prescribed flame velocities. The characteristic cellular structure of turbulent flame propagation is a correction to the flame surface area that effectively modifies the flame velocity. In general, a collection of ignition locations are specified to initiate combustion at arbitrary times. As shown in Figure 3, two ignition locations, with coordinates $\left(\hat{\zeta}^n x, \hat{\zeta}^n y, \hat{\zeta}^n z\right)$ and $\left(\hat{\zeta}^{n+1} x, \hat{\zeta}^{n+1} y, \hat{\zeta}^{n+1} z\right)$, propagate flames at separate locations. Since each ignition location ignites at a different time, the growth of the flame front resulting from each source at time, t, yields flames with radius r_n and r_{n+1}, respectively, determined by integrating over time the flame velocity associated with each source. Thus, during propagation in the volume, flames will merge and trigger additional ignition sources. Although two ignition sources are shown in this

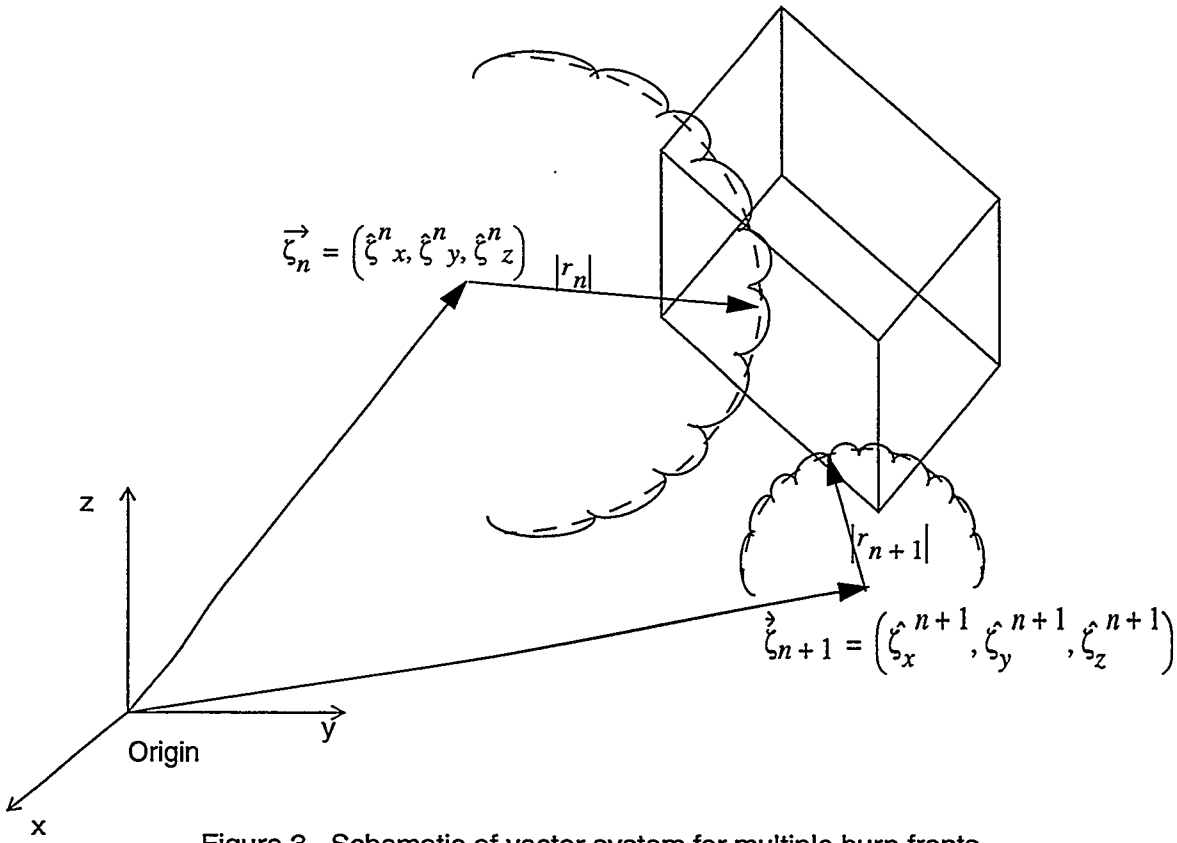

Figure 3. Schematic of vector system for multiple burn fronts.

figure, the methodology applies to any arbitrary number of ignition sources, and moreover, as the flame propagates through connected compartments of the CWT, a complex flame structure arises.

Although the following logic applies to a general polyhedron having six sides, the algorithm is described for a rectangular region of space defined by eight corner locations (See Figure 4). Thus, the square of the distance of each of these points relative to the "nth" ignition location is:

$$|R|_{i,j,k}{}^2 = (x_i - \hat{\zeta}_x^{\,n})^2 + (y_j - \hat{\zeta}_y^{\,n})^2 + (z_k - \hat{\zeta}_z^{\,n})^2 \tag{17}$$

Next, an integer value for Ψ is defined such that:

$$\text{If } (|R|_{i,j,k}{}^2 < |r_n|^2) \text{ then } (\psi_{ijk} = 1); \qquad \text{otherwise } (\psi_{ijk} = 0) \tag{18}$$

In words, if the flame front has "engulfed" the compartment point, then ψ is equal to one; whereas, if the flame front has not yet "reached" the point, then Ψ is zero. Then, a counter for all connecting points of the rectangular space is denoted as D_{ijk} which is a summation of Ψ over the polyhedron space:

$$D_{ijk} = \psi_{i,j,k} + \psi_{i+1,j,k} + \psi_{i,j+1,k} + \psi_{i,j,k+1} + \psi_{i+1,j,k+1} + \psi_{i+1,j+1,k+1} + \psi_{i+1,j+1,k} + \psi_{i,j+1,k+1} \tag{19}$$

If all of the points in the compartment are "engulfed" by the flame front, then $D_{ijk} = 8$ and the burn volume is expanded as: $V_b = V_b + V_{\text{rectangular volume}}$. If none of the points are in the flame front, then $D_{ijk} = 0$, the flame front has not yet reached this volume, and the burn volume is not updated. If D_{ijk} is between 1 and 7, then grid refinement of this compartment is performed. The rectangular region is subdi-

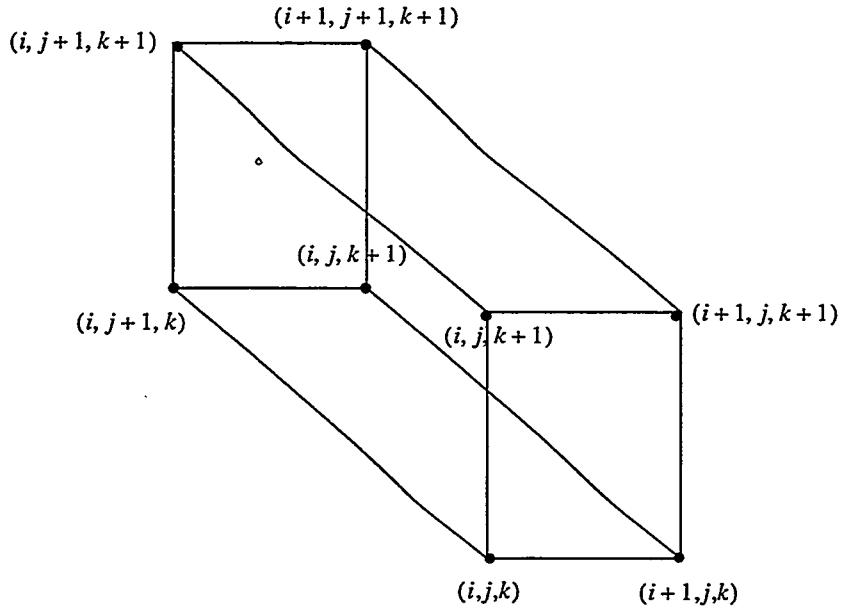

Figure 4. i, j, k designation scheme for the compartment.

vided into N_x-1, N_y-1, N_z-1 cells using a coordinate system designated as $\varsigma_i, \xi_j, \theta_k$ space (see Figure 5). The following definitions apply:

$$\Delta\varsigma = (\Delta x_i)/(N_x-1); \quad \varsigma_i = x_i + \frac{(i-1)}{(N_x-1)}\Delta x_i; \quad \mathrm{i} = 1,N_x$$

$$\Delta\xi = (\Delta y_j)/(N_y-1); \quad \xi_j = y_j + \frac{(j-1)}{(N_y-1)}\Delta y_j; \quad \mathrm{j} = 1,N_y \tag{20}$$

$$\Delta\theta = (\Delta z_k)/(N_z-1); \quad \theta_k = z_k + \frac{(k-1)}{(N_z-1)}\Delta z_k; \quad \mathrm{k} = 1,N_z$$

After the adaptive refinement of each subdivided polyhedron, the square of the distance at each corner location relative to the "nth" ignition source is defined:

$$|R|_{i,j,k}{}^2 = (\varsigma_i - \hat{\zeta}_x{}^n)^2 + (\xi_j - \hat{\zeta}_y{}^n)^2 + (\theta_k - \hat{\zeta}_z{}^n)^2 \tag{21}$$

and the integer logic variable ϕ is:

$$\text{If } (|R|_{i,j,k}{}^2 < |r_n|^2) \text{ then } (\phi_{ijk} = 1); \qquad \text{otherwise } (\phi_{ijk} = 0) \tag{22}$$

Similar to the previous logic, a summation of these integers is defined as β_{ijk} and is dependent on ϕ such that:

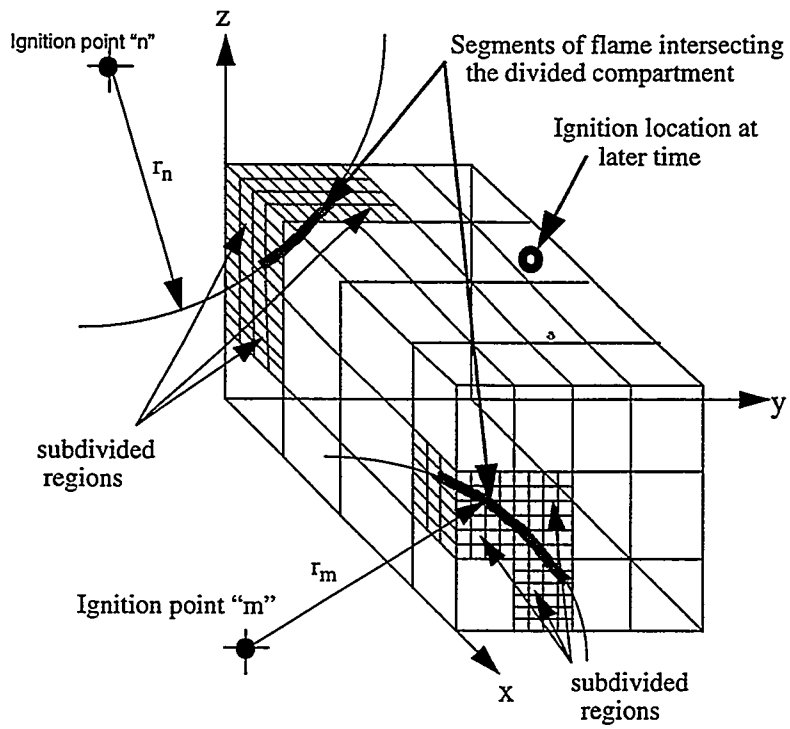

Figure 5. Adaptive mesh refine at flame surfaces to resolve effective flame area and burn volume.

$$\beta_{ijk} = \phi_{i,j,k} + \phi_{i+1,j,k} + \phi_{i,j+1,k} + \phi_{i,j,k+1} + \phi_{i+1,j,k+1} + \phi_{i+1,j+1,k+1} + \phi_{i+1,j+1,k} + \phi_{i,j+1,k+1} \tag{23}$$

and the burn volume, V_b, is updated with the expression:

$$V_b = V_b + (\Delta\varsigma\Delta\xi\Delta\theta\ \beta_{ijk})/8\,. \tag{24}$$

Estimation of the flame surface area also requires use of the integer quantity ϕ. For each of the twelve edges of the subdivided region, another integer quantity F is needed. F corresponds to twelve edges of a subdivided cell. Specifically, these are given below as:

$$\begin{aligned}
F_1 &= (\phi_{ijk} + \phi_{i+1,j,k})(2 - \phi_{ijk} - \phi_{i+1,j,k}) \\
F_2 &= (\phi_{ijk} + \phi_{i,j+1,k})(2 - \phi_{ijk} - \phi_{i,j+1,k}) \\
F_3 &= (\phi_{ijk} + \phi_{i,j,k+1})(2 - \phi_{ijk} - \phi_{i,j,k+1}) \\
F_4 &= (\phi_{i+1,j,k} + \phi_{i+1,j,k+1})(2 - \phi_{i+1,j,k} - \phi_{i+1,j,k+1}) \\
F_5 &= (\phi_{i+1,j,k} + \phi_{i+1,j+1,k})(2 - \phi_{i+1,j,k} - \phi_{i+1,j+1,k}) \\
F_6 &= (\phi_{i+1,j,k+1} + \phi_{i,j,k+1})(2 - \phi_{i+1,j,k+1} - \phi_{i,j,k+1}) \\
F_7 &= (\phi_{i+1,j,k+1} + \phi_{i+1,j+1,k+1})(2 - \phi_{i+1,j,k+1} - \phi_{i+1,j+1,k+1}) \\
F_8 &= (\phi_{i,j,k+1} + \phi_{i,j+1,k+1})(2 - \phi_{i,j,k+1} - \phi_{i,j+1,k+1}) \\
F_9 &= (\phi_{i,j+1,k} + \phi_{i+1,j+1,k})(2 - \phi_{i,j+1,k} - \phi_{i+1,j+1,k}) \\
F_{10} &= (\phi_{i,j+1,k} + \phi_{i,j+1,k+1})(2 - \phi_{i,j+1,k} - \phi_{i,j+1,k+1}) \\
F_{11} &= (\phi_{i+1,j+1,k} + \phi_{i+1,j+1,k+1})(2 - \phi_{i+1,j+1,k} - \phi_{i+1,j+1,k+1}) \\
F_{12} &= (\phi_{i,j+1,k+1} + \phi_{i+1,j+1,k+1})(2 - \phi_{i,j+1,k+1} - \phi_{i+1,j+1,k+1})
\end{aligned} \tag{25}$$

Having defined the above logic indicators, the orientation of the flame segment is determined by geometric construction and the flame surface area within the sub-volume is:

$$\begin{aligned}
A_f = {} & 0.25\omega_\beta(F_1 + F_6 + F_9 + F_{12})\Delta\xi\Delta\theta\ + \\
& 0.25\omega_\beta(F_2 + F_5 + F_7 + F_8)\Delta\varsigma\Delta\theta\ + \\
& 0.25\omega_\beta(F_3 + F_4 + F_{10} + F_{11})\Delta\varsigma\Delta\xi
\end{aligned} \tag{26}$$

The coefficient ω_β is a geometric probability related to the flame sheet orientation determined as a function only of E_{ijk}. This quantity, determined by geometry constructions, is given as; $\omega_\beta = 0$ if $\beta_{ijk} = 0, 8$, $\omega_\beta = 1/(2\sqrt{3})$ if $\beta_{ijk} = 1, 7$, $\omega_\beta = 1/\sqrt{2}$ if $\beta_{ijk} = 2, 6$, $\omega_\beta = 3/(2\sqrt{5})$ if $\beta_{ijk} = 3, 5$ and $\omega_\beta = 1$ if $\beta_{ijk} = 4$. Several simple cases of interface construction having exact val-

5.0 Flame and Burn Velocities

Consistent with the assumptions outlined in Section 2, the propagation of a turbulent flame sheet is prescribed based on experimental correlations taken from the literature [12]. This approach corrects the laminar burn velocity to account for the effects of variable unburned pressure, temperature, and turbulent flow characteristics. The temperature and pressure corrections, with exponents $\mathcal{N} = 0.2$ and $\mathcal{M} = 0.2$, are first applied as correction factors:

$$T_{corr} = \left(\frac{T}{T_{ref}}\right)^{\mathcal{N}}$$
$$P_{corr} = \left(\frac{P}{P_{ref}}\right)^{\mathcal{M}} \qquad (27)$$
$$v_f^{lam} = v_0 T_{corr} P_{corr}$$

The effects of turbulence that distort the flame sheet surface are also included as a multiplicative correction to the laminar burn velocity, $v_f = v_f^{lam}\left(v_f^{tur}/v_f^{lam}\right)$. Experimental measurement of turbulent flame speed for various gaseous fuel/air mixtures indicate that the burn velocity scales with the local turbulent intensity, (*i.e.* a rms of the fluctuating unburned gas velocity $u = \sqrt{\overline{u'_i u'_i}/3}$), and the turbulent Reynolds number, based on the intensity and integral scale l_m of the unburned gases, *(i.e.* $Re' = ul_m/\nu_g$ where ν_g is the unburned gas kinematic viscosity which, for air, has a value of 0.157 cm^2/s).

As the flame propagates through the tank volume, gas is pushed ahead of the flame and localized jet flow occurs at all of the passages connecting compartments within the CWT. This effect generates turbulence of the unburned gases leading to accelerated rates of combustion [13]. Within individual compartments, turbulent flow characteristics are determined by area-averaging the jet inflows to the region. The isotropic turbulent flow characteristics for individual jets are estimated using the classical similarity scaling laws for turbulent round jets (see Figure 6).

Turbulent jet flows form at the openings characterized by an orifice diameter, d, and the pressure difference between compartments is used to define the jet velocity, u_p. As the flow expands axially from the opening, at a given z spatial location, turbulent jet velocity fluctuations, u_z', vary in the radial direction, r, with Gaussian profile having a maximum velocity at the center denoted by $U_{z_{max}}$. Extensive experimental measurements have shown that similarity follows a dimensionless scaling variable, $r/(z-a)$, where *a* is a standoff distance from the jet origin. The Gaussian velocity distribution is described by:

$$\frac{u_z'}{(U_z)_{max}} = A\exp\left(-\lambda\left[\frac{r}{z-a}\right]^2\right). \qquad (28)$$

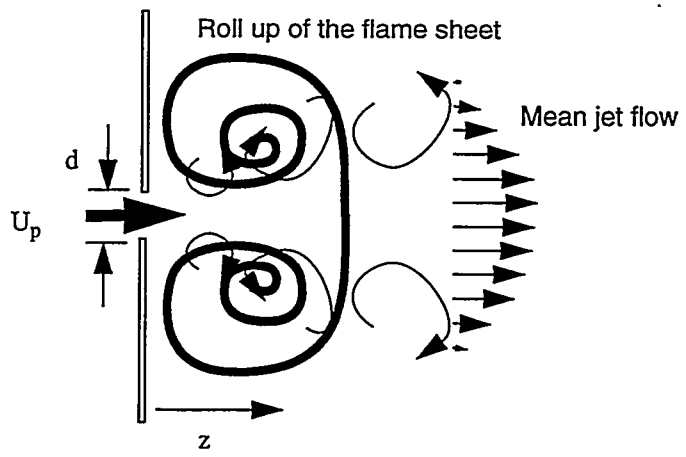

Figure 6. Turbulent jet flow through a flow passage in the walls of the compartments.

For round free jets, *A* varies between 0.2 and 0.3; hence a value of 0.25 is used in this work. From experimental measurements the standoff distance is approximately $a = d/2$, and the rate of decay is $\lambda = 22$.

Based on the assumption of isotropic turbulent flow, the turbulent kinetic energy is then:

$$k(r,z) \cong \frac{3}{2}(u')^2 \cong \frac{3}{2}(U_z)^2_{max}(0.25)^2 \ \exp\left[-2\lambda\left(\frac{r}{z-a}\right)^2\right] \tag{29}$$

and the average turbulent intensity is then defined by integrating over the radius of the jet yielding:

$$\langle k(z)\rangle = \frac{\int_0^\infty k \ (dr)}{2r_{1/2}} = \frac{3(U_z)^2_{max}d^2}{(z-d/2)^2} = \frac{3U_p^2 d^2}{(z-d/2)^2}, \tag{30}$$

where the half-width radius of the jet, $r_{1/2}$, is experimentally observed as: $r_{1/2} = 0.08(z-d/2)$ [14]. Since multiple jets are expected to be formed within each compartment, a flow area average of the jets with inflow to the compartment is used and the penetration depth of the jets, $z_{\text{compartment}}$, is bounded by the cube root of the burn volume within the compartment and the length of the potential core of the jet:

$$\begin{aligned} z_{\text{compartment}} &= max(3d, V_b{}^{1/3}{}_{\text{compartment}}) \\ d_{\text{compartment}} &= \left(\sum_i A_{\text{orifice}}\right)^{0.5}\sqrt{\frac{2}{\pi}} \\ U_p &= \frac{\sum_i (A_{\text{orifice}} v_{\text{orifice}})}{\sum_i A_{\text{orifice}}} \end{aligned} \tag{31}$$

The integral scale of the turbulent flow also follows from experimental observations, thus, $l_m = 0.21 r_{1/2}$. Based on these estimates of the turbulence flow characteristics of the unburned gases for each compartment, the Reynolds number, Re' and turbulent intensity provide the input for determining the turbulent flame velocity given in functional form:

$$V_f^{turb}/V_f^{lam} = 1.0 + 5.4\frac{(0.25 + Re'/1250.)}{(1.0 + Re'/1250.)}\left(\frac{u'}{V_f^{lam}}\right)^{0.5} + \frac{(2.0 + (Re'/1250.)^{0.5})}{(1.0 + Re'/1250.)}\sqrt{1.0 - \frac{1.0}{\left(1.0 + 0.75\left(\frac{u'}{V_f^{lam}}\right)^{0.5}\right)}} \quad (32)$$

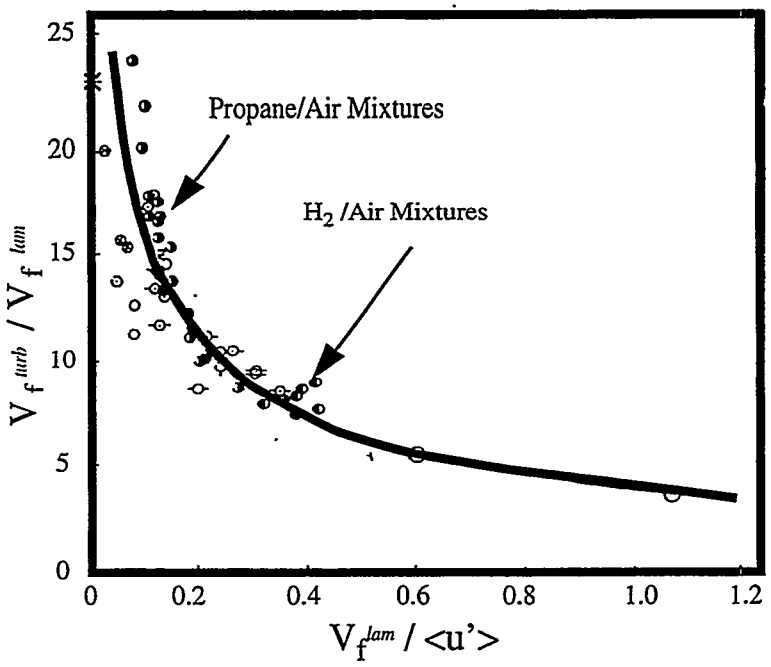

Figure 7. Experimental measurements of the ratio of turbulent flame speed to laminar flame speed at various levels of turbulent intensity.

Figure 7 displays experimental measurements of the ratio of the turbulent flame speed to the laminar value vs. the inverse of scaled turbulent intensity for reacting gaseous flows with Re' ~ 2000 [12]. Turbulent flame speed is roughly a factor of ten greater than that of the laminar flame speed.

Given an estimate of the turbulent flame velocity of propagation, the burn velocity in Equation 15 includes the effect of mean flow at the flame front. To leading order, for one-dimensional flow, the normal velocity ahead of the flame is approximately

$$v_u \sim \frac{V_u}{\gamma_u A_f p} \frac{dp}{dt} . \tag{33}$$

Similarly, the normal velocity of the burned gases expanding away from the flame is approximately:

$$v_b \sim -\frac{V_b}{\gamma_b A_f p} \frac{dp}{dt} . \tag{34}$$

Using equations 13 and 14, the flame velocity is then related to the burn velocity by

$$\mathcal{V}_f \cong \mu \left\{ \frac{E V_u/\gamma_u + V_b/\gamma_b}{V_u/\gamma_u + V_b/\gamma_b} \right\} . \tag{35}$$

6.0 Heat Transfer Models

Prior experience in the modeling of flame propagation in enclosures demonstrates that heat transfer is an important effect that reduces the maximum overpressure imparted to an enclosure. During turbulent burning, there is a rapid increase in temperature and pressure followed by a decay due to the effects of heat loss. Near cold walls, local boundary layer effects lead to convective heat transfer energy losses. An additional heat loss mechanism, taking place on a volumetric scale, is the effect of thermal radiation. Typically, the products of hydrocarbon combustion form gases that are effective emitters of thermal radiation. Heat loss from both the burned region to the unburned regions and to the cold walls of the CWT is important during flame propagation in large-scale enclosures particularly when lean fuel - air mixtures are considered. For example, Figure 2, shows a comparison between ideal equilibrium isochoric combustion predictions and experimental observations. Ideal combustion calculations overpredict the pressure rise in the enclosure.

6.1 Radiative heat transfer

To model the effects of thermal radiation in an enclosure, the walls are assumed to be cold blackbody surfaces; hence, the wall radiative transfer to the reacted gases is neglected. Consistent with engineering heat transfer models, the rate of heat loss from the burned gases and the absorption of thermal radiation by the unburned gases is based on an equivalent isothermal temperature (a volumetric average value for the burned and unburned regions in each compartment) and a mean beam length for each compartment. Emission and absorption coefficients are computed using appropriate molecular band models for H_2O, CO_2 and CO. The rate of energy loss from the combustion gases is determined by the thermal radiation emitted in the burned volume within each compartment. In a similar manner, the rate of energy transfer to the unburned gases is taken as that fraction of the radiant energy which passes through the flame surface and is absorbed by the unburned volume of each compartment. A determination of the absorption coefficient within the unburned gases establishes the energy that can be absorbed by the cooler unburned gases. The remaining energy from the combustion region is transmitted and lost to the enclosure walls. In addition to the flame surface area, the flame propagation algorithm determines the area of the enclosure walls that are covered by burned gases and the thermal energy is distributed accordingly.

During propagation, isobaric equilibrium calculations are performed to determine appropriate concentrations of H_2O, CO_2 and CO. Rather than integrating over all wavelengths, it is assumed that significant energy absorption of each species occurs in several bandwidths. This assumption greatly simplifies the radiation model. For the sake of brevity, the details of the exponential wide-band model can be found in the monograph by D. K. Edwards on molecular gas band radiation [8].

6.2 Convective heat transfer

Near the wall surface, there is an additional heat transfer effect due to the turbulent flow of hot gases in boundary layer regions. Consistent with engineering analysis, convective heat transfer is modeled by Newton's law of cooling whereby the energy flux to a cold surface is proportional to the temperature difference between the surface and the surrounding medium such that $\dot{\vec{q}}_{con} = \mathcal{H}(T_b - T_w)$ where T_b is the temperature of the burned gas in each compartment, T_w is the wall temperature and $\mathcal{H}$ is the coefficient of surface heat transfer. Typically, this coefficient is a function of geometry and flow conditions. This mode of heat transfer has a secondary influence so the heat transfer coefficient is treated as a constant and determined empirically by replicating the decay rate of the pressure following complete combustion within the enclosure.

7.0 Flow Between Compartments

In modeling the flow between compartments, an engineering model for orifice flow is used. Thus, the flow rate is dependent on the pressure ratio of the connected compartments. For a condition where $P_1 > P_2$ inflow to compartment 2 occurs corresponding to the outflow of compartment 1. A bound on the flow is constrained by a critical pressure ratio:

$$\left(\frac{P_1}{P_2}\right)_{crit} = \left(\frac{\gamma+1}{2}\right)^{\gamma/(\gamma-1)} \tag{36}$$

where γ is the specific heat ratio. The mass flow is then described by:

$$\text{If } \frac{P_1}{P_2} > \left(\frac{P_1}{P_2}\right)_{crit}, \text{ then } \dot{m} = C_d A_{or} P_1 \sqrt{\frac{\gamma}{RT_1}\left(\frac{2}{\gamma+1}\right)^{\frac{\gamma+1}{\gamma-1}}}$$

$$\text{otherwise, } \dot{m} = C_d A_{or} P_2 \sqrt{\frac{2\gamma}{RT_1}\left(\frac{1}{\gamma-1}\right)\left(\frac{P_1}{P_2}\right)^{\frac{(\gamma-1)}{\gamma}}\left(\left(\frac{P_1}{P_2}\right)^{\frac{(\gamma-1)}{\gamma}} - 1\right)} \tag{37}$$

where C_d is the discharge coefficient, taken to be a constant value of 0.65, $\dot{m}$ is the mass flow rate, and A_{or} is the cross-sectional area of the orifice. To determine the flow direction, the compartment pressures are monitored to ensure that P_1 is greater than P_2. Additional modifications have been put in place to allow arbitrary coupling of the compartments to allow the effects of gas venting in the CWT through fuel line stringers. At each "orifice" location, ignition sources are also placed which allows flame propagation between the compartments.

In reviewing this modeling, it is noted that the geometry and the logic associated with the propagation of turbulent flames throughout the CWT involves a very complex system model. As an illustration of the complex nature of the flame propagation, Figure 8 displays a typical set of time planes for accelerated flame propagation into the six-compartment tank geometry displayed in Figure 1. As is seen in this figure, multiple combustion waves form as a result of propagation at multiple flow openings within the partitions separating the tank. Although many simplifications have been introduced in this modeling, the predictability of the model can be compared to actual experimental measurements. Hopefully, a reasonable level of predictability can be established with this approach so that this modeling can be incorporated in mechanics analysis for coupled combustion/damage predictions of the full-scale geometry.

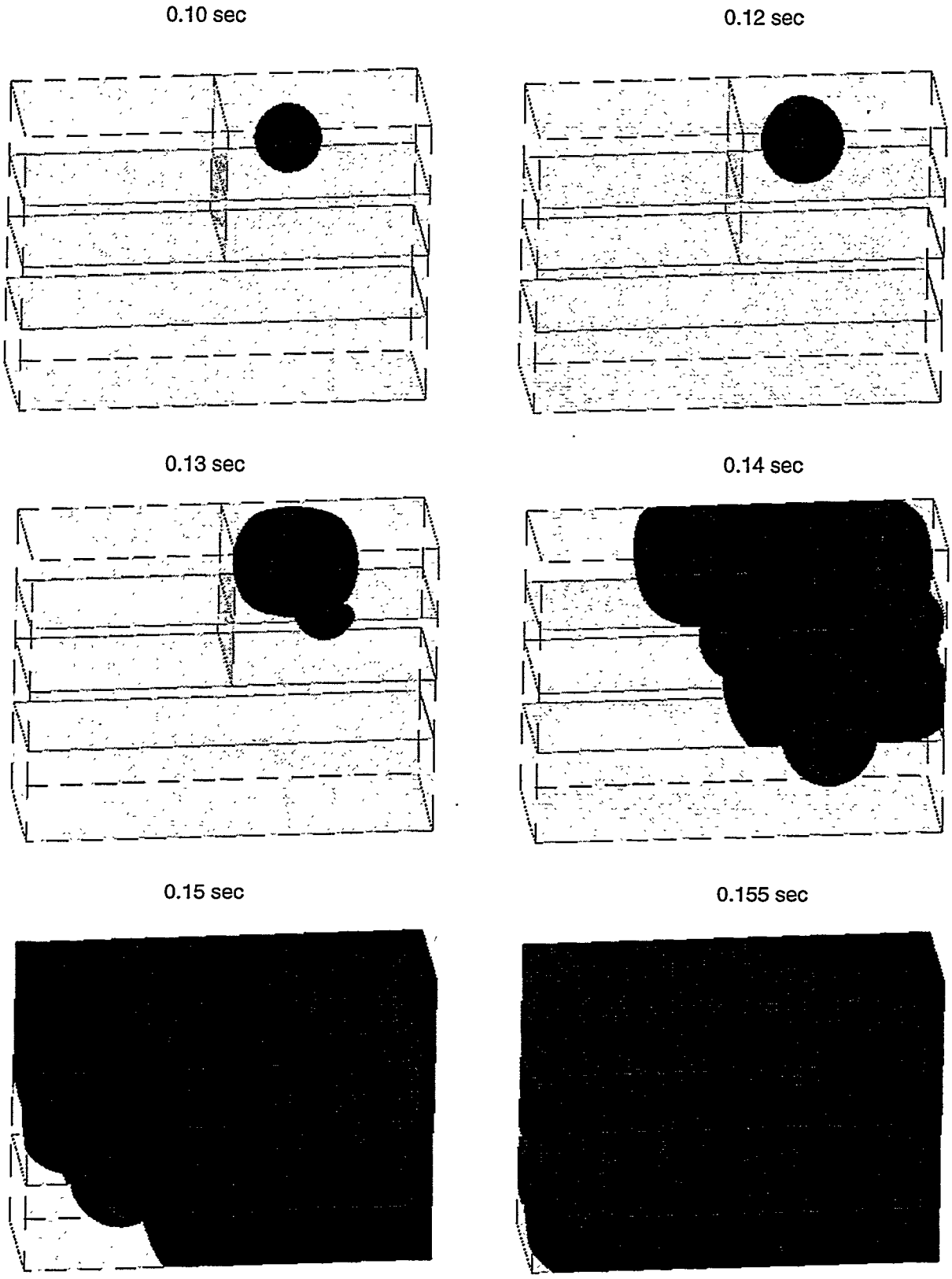

Figure 8. A typical calculation showing select time planes of the flame propagation during accelerated combustion.

8.0 Simulation Results and Comparison to Experiments

8.1 The HYJET Experiment

In the early planning stages of the experimental testing program, a simulant gas fuel mixture was considered to replace the Jet A fuel. Since Jet A fuel is a distilling cut composed of a blend of light and heavy hydrocarbon components, its exact composition varies from supplier to supplier. Controlling the fuel/air stoichiometry from test to test is then exceedingly difficult, particularly in tests conducted with environmental changes. Additionally, if the Jet A fuel has to be heated, safety concerns become an important factor. In determining a fuel simulant, various propane/hydrogen fuel mixtures were tested in the CalTech HYJET Facility.

A schematic of the HYJET test chamber is shown in Figure 9. A fuel-air mixture consisting of 7% hydrogen, 1.4% propane and 91.6% air at 0.83 bar has been found to reproduce maximum pressure and rise rate similar to that of a mixture of Jet A and air representative of aircraft fuel-air mixtures that could have existed in TWA 800. This fuel-air testing provides a set of single-compartment test data needed to determine the flame velocities for the modeling of the quarter-scale tests.

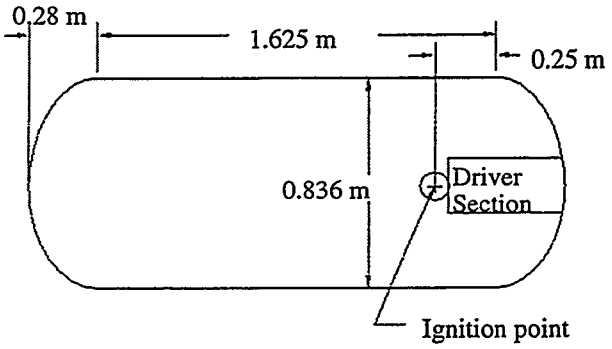

Figure 9. Experimental configuration for HYJET combustion apparatus.

In modeling the HYJET tests, the cylindrical tank volume occupying 1.18 m^3 is replaced by a rectangular volume having dimensions 203 cm by 76.2 cm by 76.2 cm, preserving the combustion volume and the cross-sectional area of the tank. Figure 10 compares the experimental measurement of the transient overpressure and computed results for HYJET Test 493. Similar to the experimental measurements, the early time behavior is indicative of spherical wave growth; as the flame interacts with the walls of the confinement, an inflection in the pres

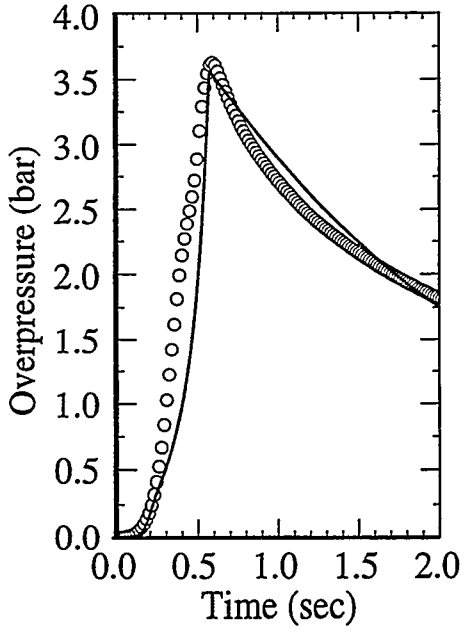

Figure 10. Experimental and calculational results for HYJET Test 493.

sure time history is seen. The small differences in calculated vs. experimental are due to differences in the cross-sectional area. Nonetheless, the burn time and magnitude of peak overpressure are reasonably well-predicted. Similarly, the cool-down of the combustion gases occurs after a burn time of 0.6 seconds and is also fairly well-modeled. Overall, the lab-scaled tests provided a valuable single compartment benchmark. In particular, the HYJET work provided confidence in the modeling approach, and also demonstrated the importance of accounting for heat transfer.

8.2 The Quarter-Scale Experimental Tests

Thirty tests were conducted over the course of several months in a one-quarter scale test set-up of the CWT configuration. In sixteen of these tests, referred to as "weak" configurations, one or more of the compartment partitions purposely failed during the test. In these tests, structural mechanics aspects occur during combustion and the loss of confinement has a significant effect on the overpressure within the tank confinement during the time of flame acceleration. The effects of structural failure of the confinement is not considered in the current modeling. A limited set of tests (14) considered combustion in a rigid confinement; these are suitable to comparison with modeling. Of these tests, three are excluded due to instrumentation and ignition problems. Test 1 used a pyrotechnic match ignition source that produced incendiary burning fragments throughout the compartment. The mode of ignition in this test is not well defined. In Test 2 the instrumentation experienced noise corruption in the pressure measurements. Test 3

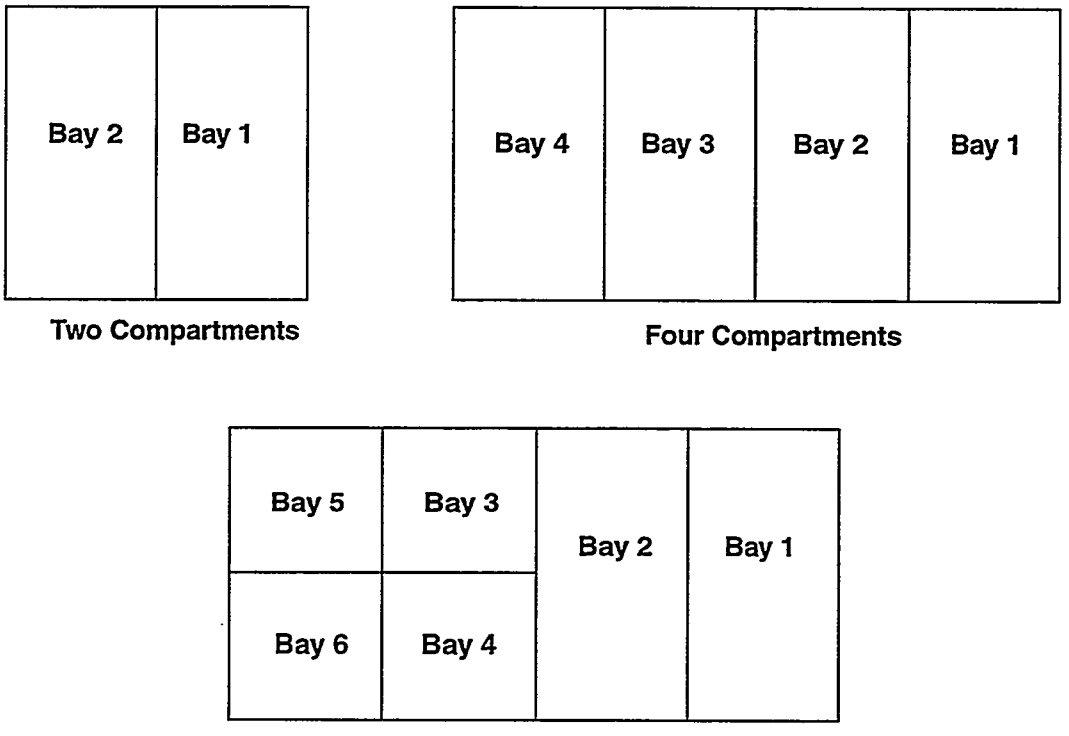

Figure 11. Compartment numbering system for various configurations.

was conducted to verify that the backup ignition source was operational; unfortunately, the two ignition sources inadvertently ignited leading to multiple flames. Thus, only eleven of the thirty tests are appropriate for comparison to the combustion model with rigid confinement. Consistent with the numbering scheme used in the testing, the quarter-scale configuration is shown in Figure 11. In the CWT of the Boeing 747, there is an additional dry empty compartment between bay 1 and the cargo hull. This compartment is denoted as compartment 0. Since the modeling did not include any mechanics effects, the dry compartment was not included in the simulations. In all of the tests, the gaseous mixture initially consists of 1.4% propane, 7.0% hydrogen, and 91.6% air. All eleven tests used a single ignition source. The number of compartments, number of orifices, whether venting was allowed, and the location of the single ignition source are varied in these test series, as given in Table 1.

Table 1. Matrix of experimental tests that were computationally modeled.

Test#	# Compartments	Vented	Ign Location	# Orifices*
4	6	yes	5	49
5	6	yes	3	49
6	6	yes	2	49
7	6	yes	1	49
8	6	yes	5	49
9	4	no	5	27
10	2	no	5	10
11	1	no	5	0
12	2	no	5	1
15	6	yes	6R	49
16	6	yes	1R	49

The observed and calculated pressure traces of these tests exhibit three distinct characteristics: (1) an initial pressure rise where a single spherical flame kernel slowly expands from the ignition source; (2) a transition into a turbulent mode of combustion due to generation of turbulence by jetting effects in connected compartments indicated by rapid pressure rise; and (3) after combustion takes place the pressure drops due to heat transfer effects. The time of the laminar burn is specified in the model by two parameters: a reference velocity of the laminar burn; and the volume to be consumed by the laminar flame until it transitions to a cellular structure [10]. When the flame transitions from laminar to turbulent, the flame speed is modified according to the mean turbulence properties of the flow in the compartment. To include the effects of flame cellular and flame sheet wrinkling, the flame surface area is modified. The interface algorithm calculates a flame surface area based on spherical sectors and this surface area is arbitrarily increased by a factor of 5-10% to account for cellular flame effects. Table 2 summaries the empirical

parameters used in the simulations. In Test 8, the experimental configuration includes liquid Jet A that is probably lofted and entrained into the burn region. Thus, the flame speed is enhanced to cause a more rapid pressure rise. This enhanced flame propagation is modeled by increasing the laminar burn velocity and reducing the laminar burn volume.

Table 2. Velocity and burn volume/area empirical parameters for each test.

Test#	Laminar burn velocity (cm/s)	Laminar volume (cm^3)	Burn area multiplier	Turbulent Reference Velocity (cm/s)	No. Compartments
4	110.	8000.	1.05	200.	6
5	110.	8000.	1.00	150.	6
6	85.	15000.	1.07	200.	6
7	85.	10000.	1.10	200.	6
8	200.	2000.	1.07	200.	6
9	100.	10000.	1.06	200.	4
10	85.	15000.	1.07	150.	2
11	85.	10000.	1.05	85.	1
12	110.	10000.	1.07	150.	2
15	95.	10000.	1.07	200.	6
16	95.	15000.	1.07	200.	6

Figure 12 displays a comparison of model calculations to experimental measurements of overpressure in Test 11. This is a configuration in which all of the tank panels are removed and the flame propagates in a single compartment enclosure. In this test, there are six pressure transducers to monitor the pressure throughout the compartment and the six pressure measurements are plotted as solid lines in Figure 12. The model calculations are represented as a trace of circles. Since all of the pressure traces measure identical pressure histories, this verifies that the pressure within a compartment is spatially invariant consistent with the approximations involved in the modeling. In this test, the burn time to the peak pressure is approximately twice the time of the tests that include partitions. In the single compartment test, accelerated combustion occurs due to low levels of turbulence generation that is dramatically different (and slower) than turbulence levels generated by jetting effects as the combustion expands through passages in the partition walls..

Figure 13 compares the calculated versus experimental measurements of the pressure histories in a two compartment configuration (Test 10). In this test, a single partition separates two combustible regions and ten openings allow flow between the compartments. Similar to the previous comparison, the computational model replicates the pressure measurements quite well. In this test, a single source ignites the mix-

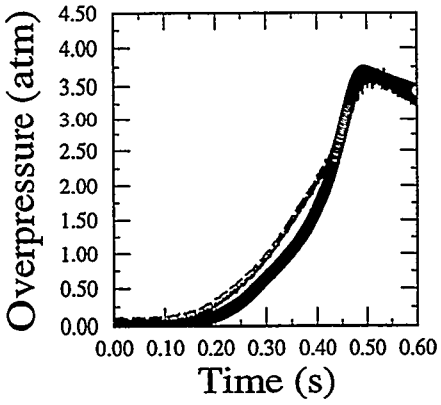

Figure 12. Overpressure versus time for Quarter-Scale Experiment 11

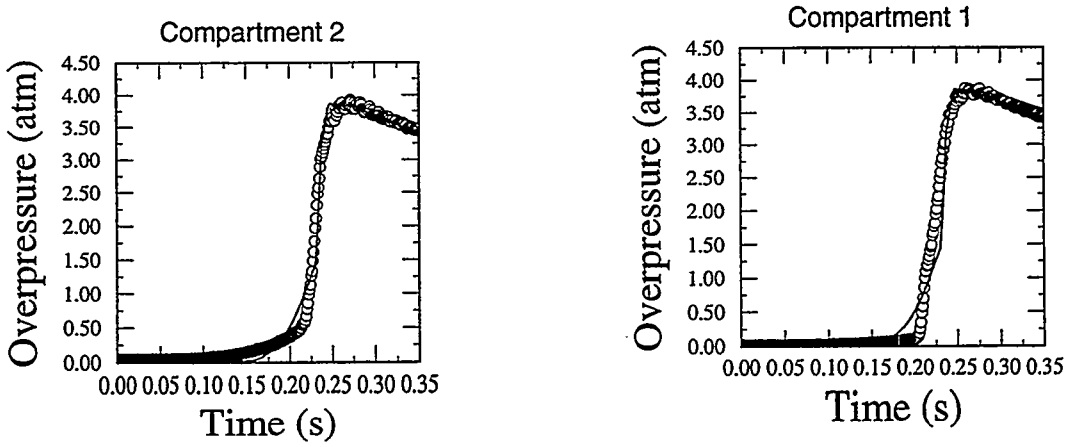

Figure 13. Overpressure versus time for Quarter-Scale Experiment 10.

ture of Compartment 2, so the flame propagated from Compartment 2 into Compartment 1. In comparison to the single compartment test of Test 11, a higher level of turbulence is generated by the jetting of gases in connected regions. As illustrated in Figure 8, after the flame impinges on the partition walls, multiple flames are formed which accelerate due to the effects of jetting flow into connected compartments.

Test 12 is another two compartment test, shown in Figure 14. However, rather than having a distributed number of openings in the partition, a single hole, with the same accumulated area, is used. A similar accelerated combustion wave occurs as the flame propagates between compartments. Since the single opening in Test 12 significantly altered the mean flow field, localized entrained flow causes the flame to propagat at a somewhat higher rate than predicted by the modeling. This is not surprising. The effects of mean flow are only approximated in this model and no attempt is made to describe detailed fluid dynamic effects. Nonetheless, the overall predictions of burn times and peak overpressure are reasonably well predicted.

Additional tests in the quarter-scale configuration correspond to a four-compartment configuration as defined in Test 9 and displayed in Figure 15. Again, all model pressure histories compare well with the ex-

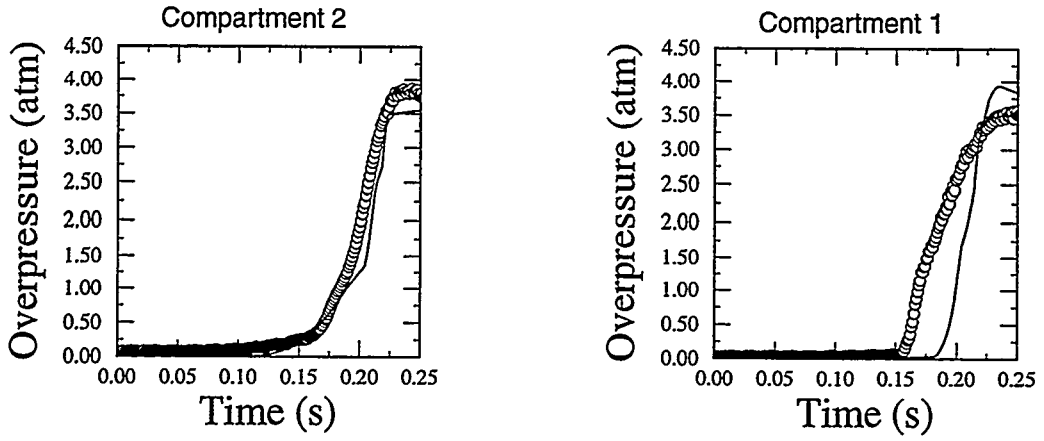

Figure 14. Overpressure versus time for Quarter-Scale Experiment 12.

perimental pressure measurements. The time scales of laminar propagation to the onset of accelerated combustion and rate of accelerated combustion as the flame propagates throughout the tank are reasonably well replicated. In overlaying these pressure profiles it is noted that the last compartment into which the flame propagates experiences a pressure piling effect causing the overpressure to be the largest in that region. The pressures then drop as the gas flows back into burned regions and cools.

The six-compartment configuration is representative of the actual fuel tank of TWA 800 CWT. In this series of tests, the ignition location is varied. Test 4 corresponds to an ignition location in compartment 5. A comparison between predicted and experimental overpressure measurements is shown in Figure 16. Although excellent agreement with the experimental overpressure in compartment 5 is seen, a somewhat higher pressure rise is predicted for Compartment 6, wheras lower pressures are predicted in the four other compartments. The prediction of the time to accelerated combustion and the drop in pressure due to heat loss during the cool-down is well described. In this test case, the "flow resistance" between Compartments 5 and 6 is apparently too low, resulting in a slighly higher overpressure in Compartment 6. The higher flow rate into compartment 6 means less flow into the remaining compartments which is reflected by differences seen in the pressure maximum. This test includes the effect of venting stringers which may have an influence in the gas mass flow between compartments.

Experiment 5 is a six-compartment configuration with an ignition location in compartment 3. In this test, the pressure transducer in compartment 1 failed, so the model and experimental results are only compared for five compartments. The model predictions of pressure in Compartment 2 replicate well the experimental measurements as seen in Figure 17. In Compartments 6 and 4, the pressure rise rates are slightly slower than observed and the peak overpressures are slightly higher than measured. However, the calculated overpressures in Compartments 5 and 3 are only slightly lower than observed. Again, this indicates that the flow restrictions at the compartment walls may need to be appropriately adjusted. However, the overall flame growth and burn rates are well predicted.

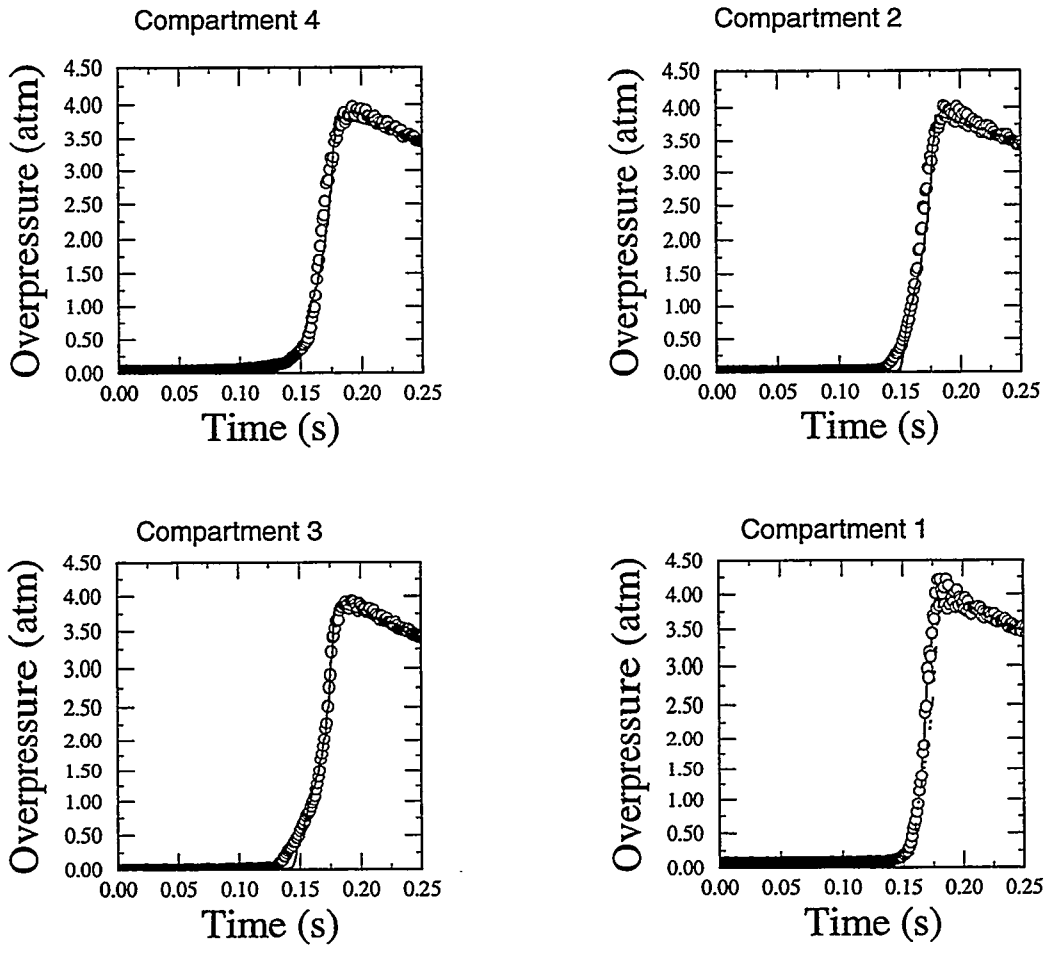

Figure 15. Overpressure versus time for Quarter-Scale Experiment 9

Experiments 6 and 7 are six-compartment configurations in which the location of the ignition source is varied. As can be observed in Figures 18 and 19, the computed results followed the trends observed for Experiment 5. In general, the initial induction time to accelerated combustion, peak overpressure and heat loss during the cool down period are reasonably well-described.

Experiment 8 is a test that includes liquid Jet A fuel on the floor of the quarter-scale tank. As suspected, liquid jet fuel is lofted into the confinement and augments the effects of turbulence generation. The experimental measurements given in Figure 20 indicate that a shorter induction time to accelerated combustion takes place. To incorporate the effects of two-phase combustion, the flame velocity is increased to shorten the burn times and the calculated pressure histories in all of the compartments are correlated. The differences in the peak pressures are probably due to added combustion of the liquid fuel during propagation. This energy release and other two-phase flow effects are not included in the model calculations.

Tests 15 and 16 correspond to the ignition locations in Compartment 6 and 1, respectively. A comparison of predicted and measured pressure histories are given in Figures 21 and 22. An interesting feature of these tests is that they have similar pressure histories. Note that the experimental pressure data for

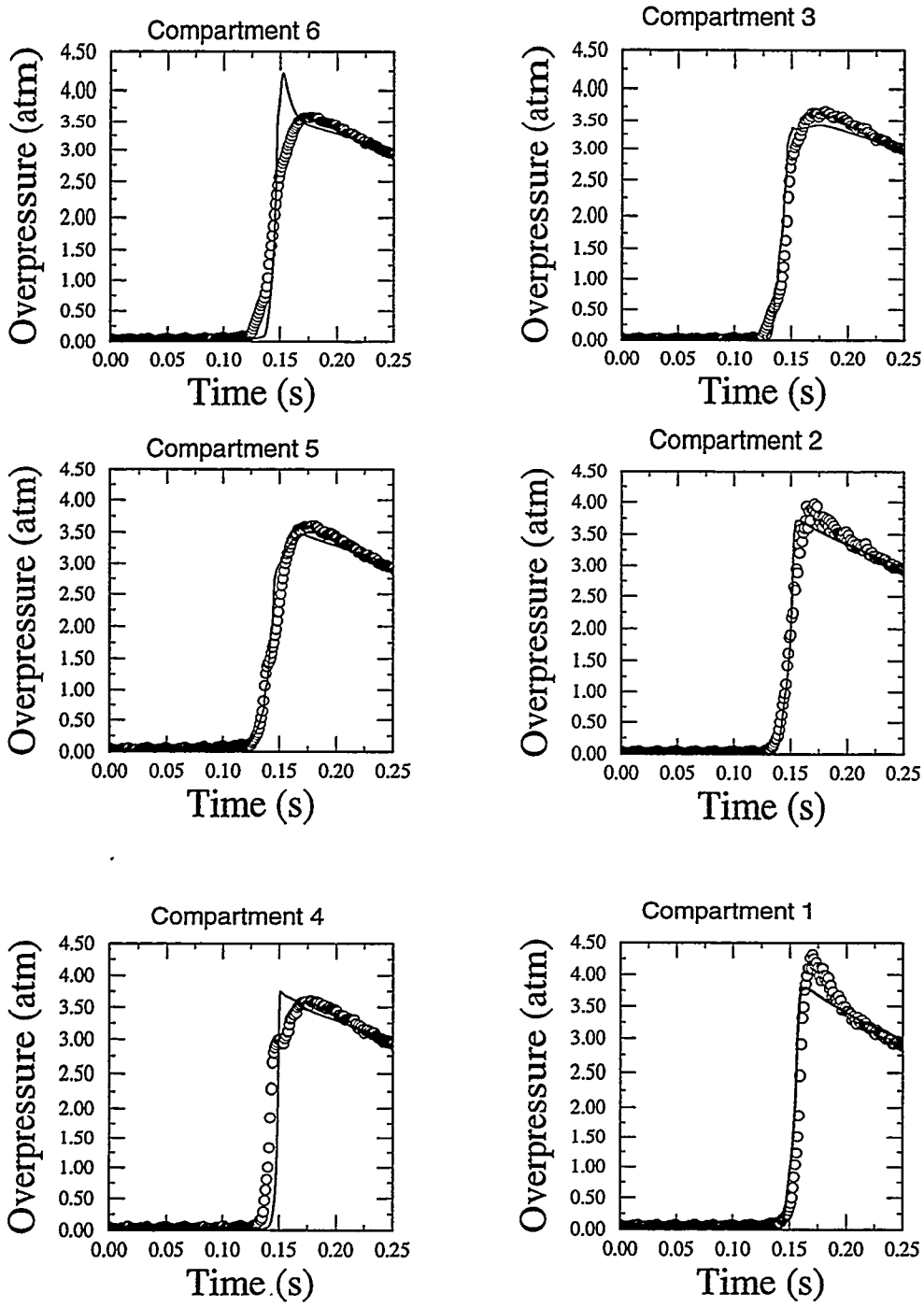

Figure 16. Overpressure versus time for Quarter-Scale Experiment 4.

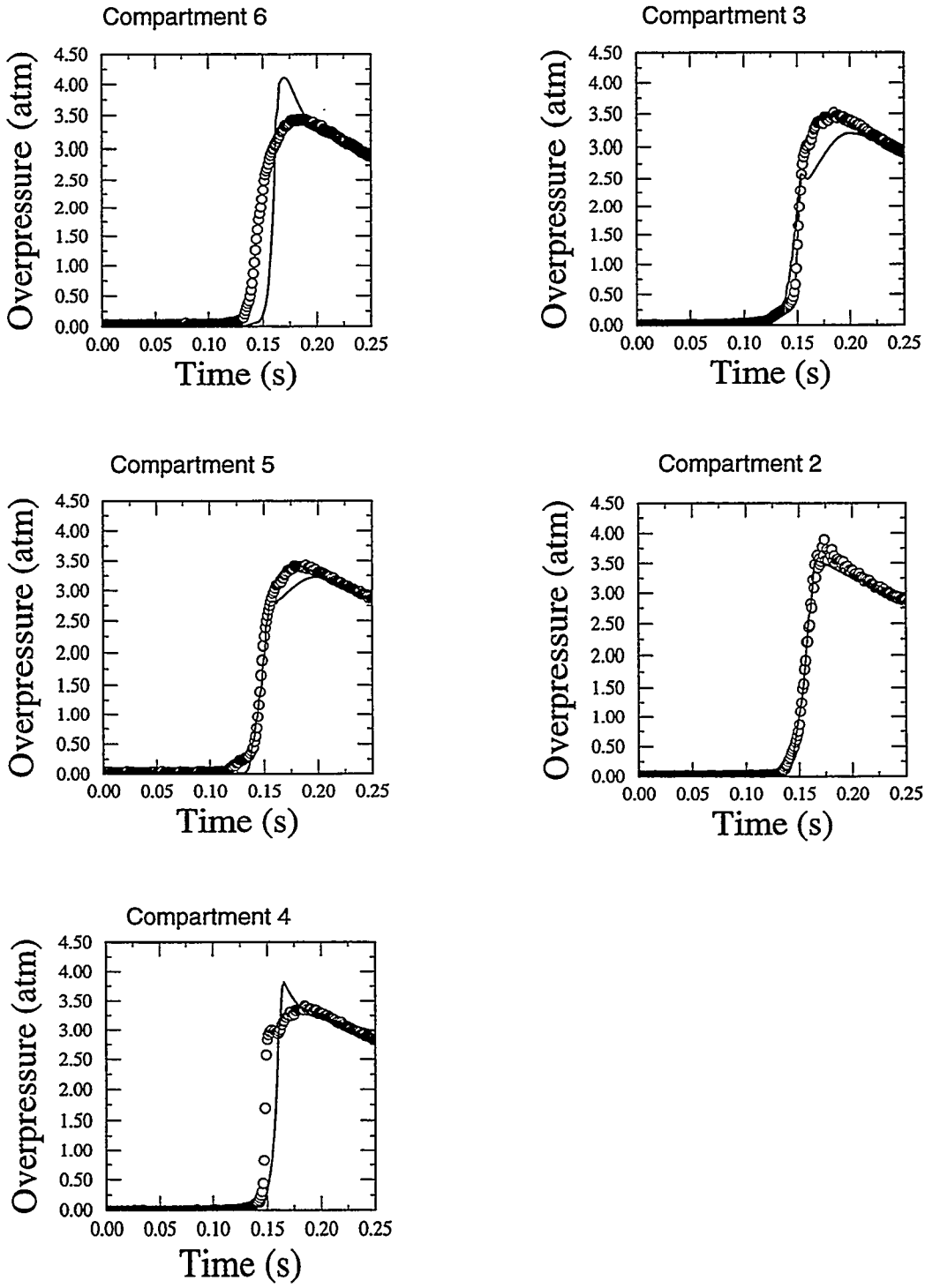

Figure 17. Overpressure versus time for Quarter-Scale Experiment 5.

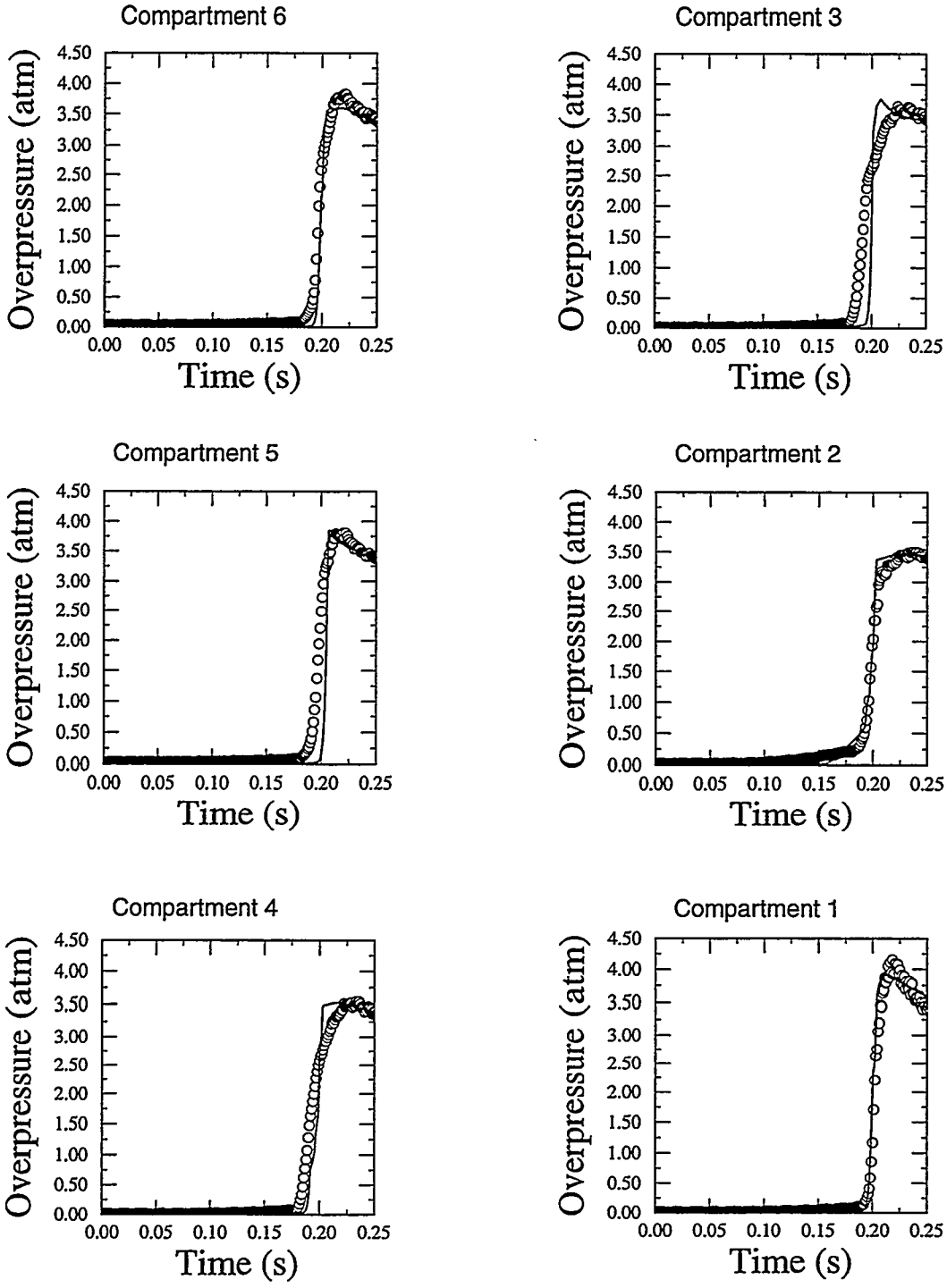

Figure 18. Overpressure versus time for Quater-Scale Experiment 6.

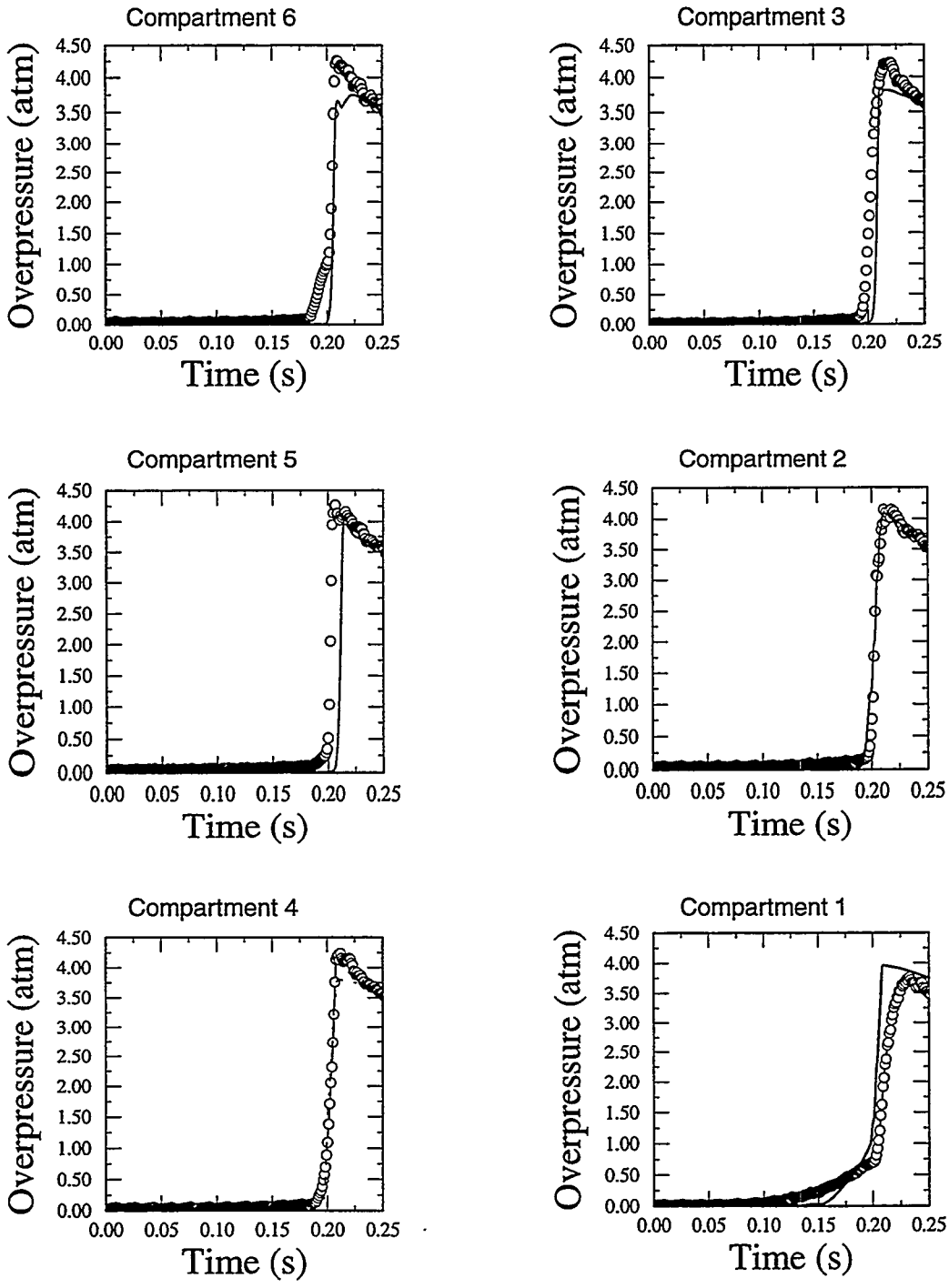

Figure 19. Overpressure versus time for Quater-Scale Experiment 7.

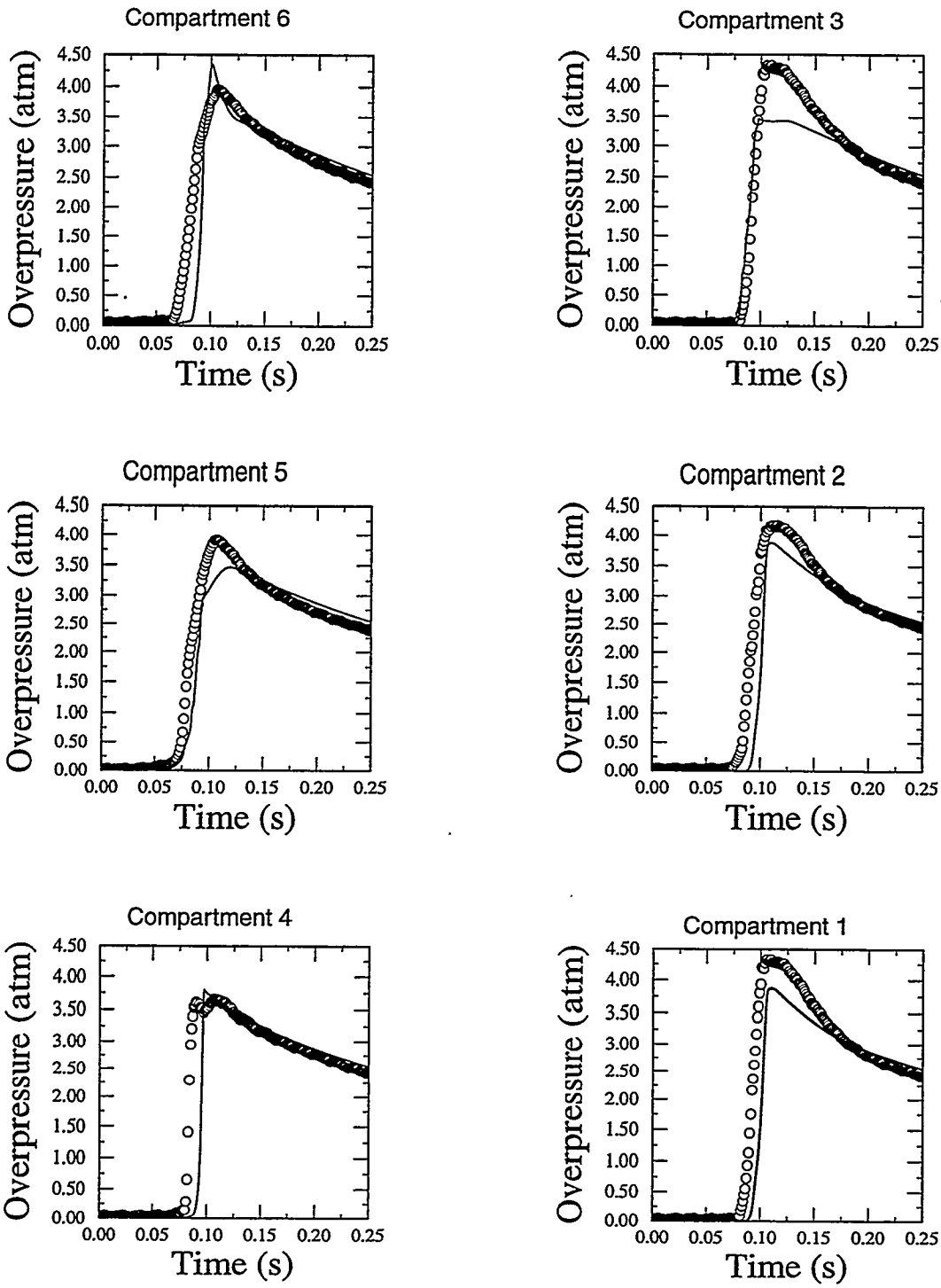

Figure 20. Overpressure versus time for Quater-Scale Experiment 8.

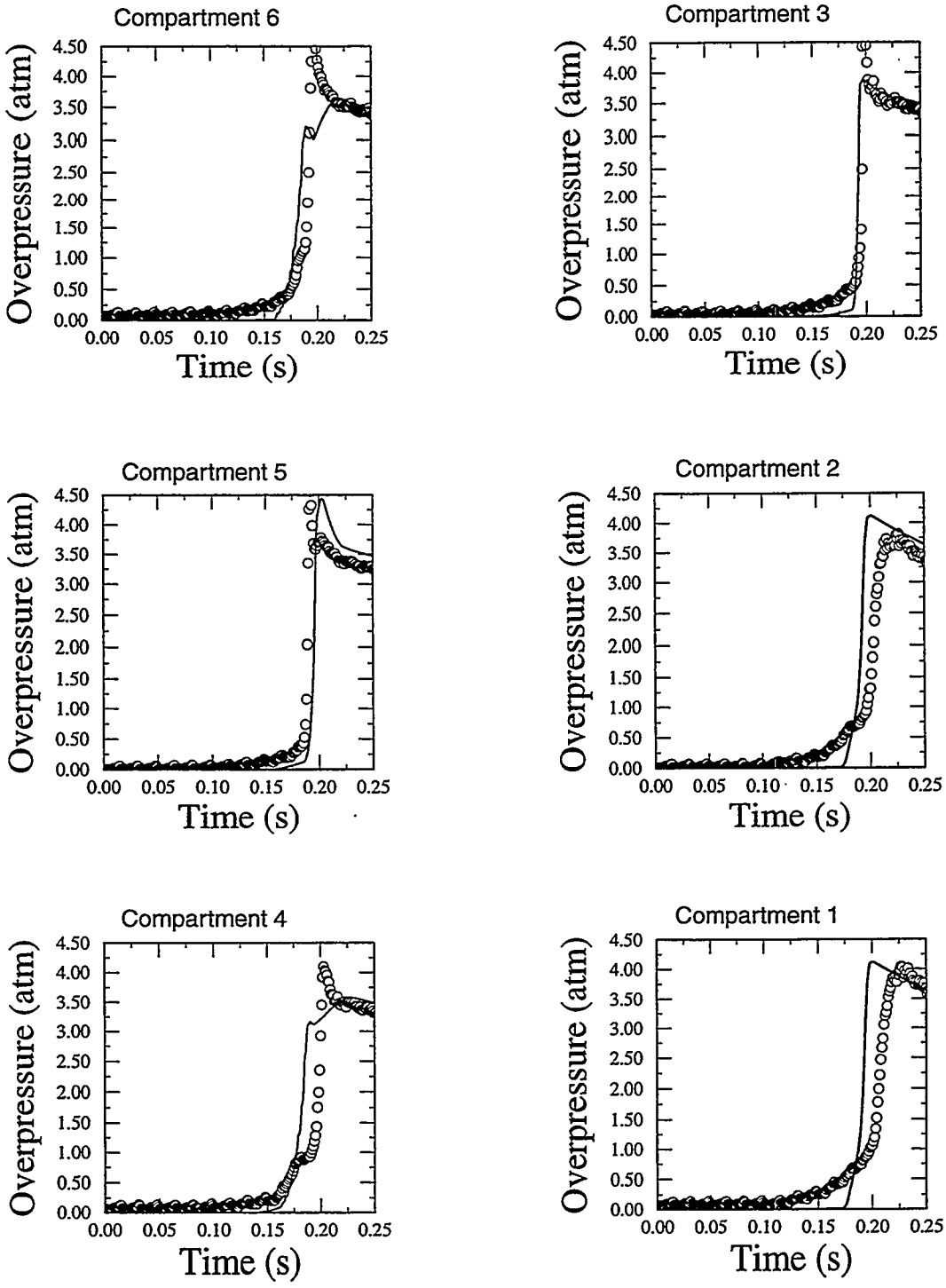

Figure 21. Overpressure versus time for Quater-Scale Experiment 15.

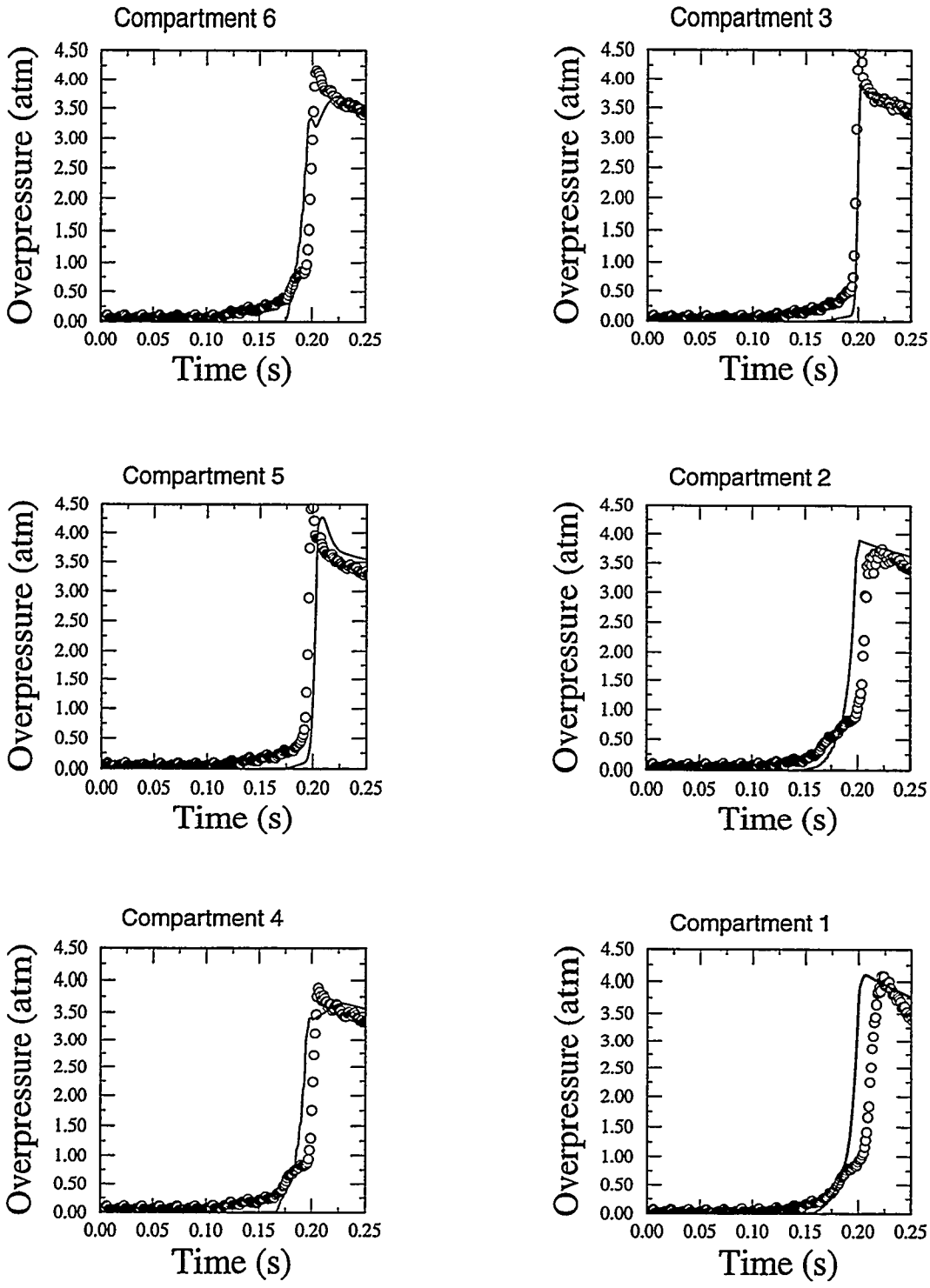

Figure 21. Overpressure versus time for Quater-Scale Experiment 16.

Compartment 4 initially rises, experiences a slight delay, and then the pressure rapidly increases. Venting to the ambient environment occurs in both of these tests. The model predictions show a similar behavior, but at a slightly later time and at a corresponding higher pressure. This effect does not occur if the stringer vents are excluded in the modeling.

9.0 Parametric Variations of Ignition Location

The NTSB determined that there are eight possible ignition locations corresponding to fuel probes and the compensator in the actual CWT. These locations are given in FIgure 23. Locations marked 1 through 7 correspond to the seven fuel probes within the tank, and location 8 is the compensator. The combustion parameters from the previously described work on the quarter-scale experiments were fixed. Then, the model was applied to study/evaluate the effects of combustion initiating at each of the eight sources . Such studies provide guidence to the follow-on experimental efforts supported by NTSB to define the actual cause and location of the ignition source. In this part of the study, the pressure differences between consecutive compartments are determined. Additionally, the impulse (integrated pressure difference over time) is determined and represented in the pressure-impulse (P-I) plane, often used in evaluating damage to structures [15].

As a result of postmortem examination of the spar wall connecting compartments 1 and 2 in the actual fuel tank, it is believeded that the combustion caused a differential pressure load that changed loading directions. In other words, the wall received an initial impulse loading and at a later time, the wall received a reverse impulse in the opposite direction, indicating that the compartment containing the highest pressure had switched from one compartment to the other.

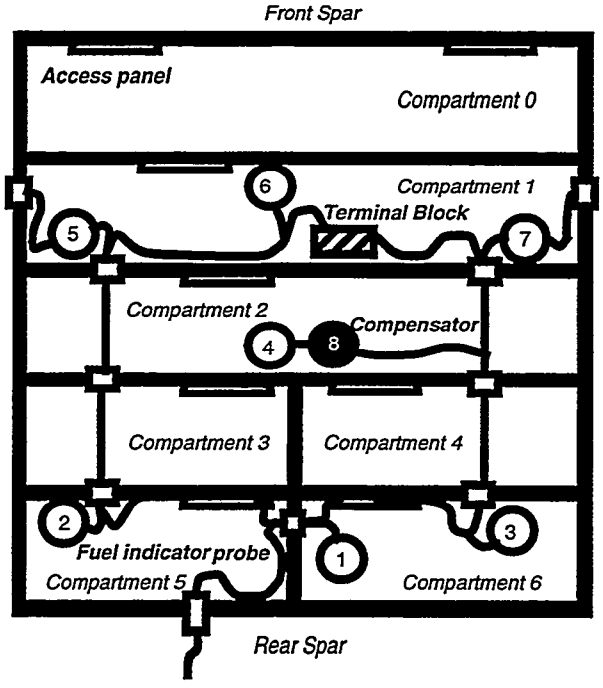

Figure 23. Locations of the eight possible ignition sources.

In the analysis to follow, the pressure difference between Compartment 1 and 2 is $p' = p_j - p_i$ and, the impulse on the compartment wall is defined as

$$I(t) = \int_{t_0}^{t_1} p'dt \tag{38}$$

Figures 24 to 31 display the pressure differences and the P-I diagrams for the partition wall between compartments 1 and 2 for each of the eight possible ignition locations. The largest pressure difference in the tank occurs between compartment 1 and compartment 0 (the dry compartment) because compartment 0 is always fixed at ambient pressure until the tank ruptures. This pressure difference is also included in these figures.

Model calculations suggest that the pressure difference for ignition Locations 1 and 2 never change sign. This strongly suggests that these locations may be eliminated as possible candidates for ignition sources in the actual incident. A combustion event initiated at location 6 produces pressure differences that eventually change sign but the delivered impulse may be insufficient to cause reversed motion of the wall. Similarly, the impulse from combustion events ignited at Locations 5 and 7 are also weak because the combustion waves arrive nearly simultaneously in Compartments 1 and 2. Finally, as the ignition location is moved to the center of the tank, the pressure difference and the impulse change sign. This strongly suggests that a potential initial location may have occurred in Locations 4 or 8. A more definitive assessment relies on coupled combustion and structural failure analysis that should be pursued.

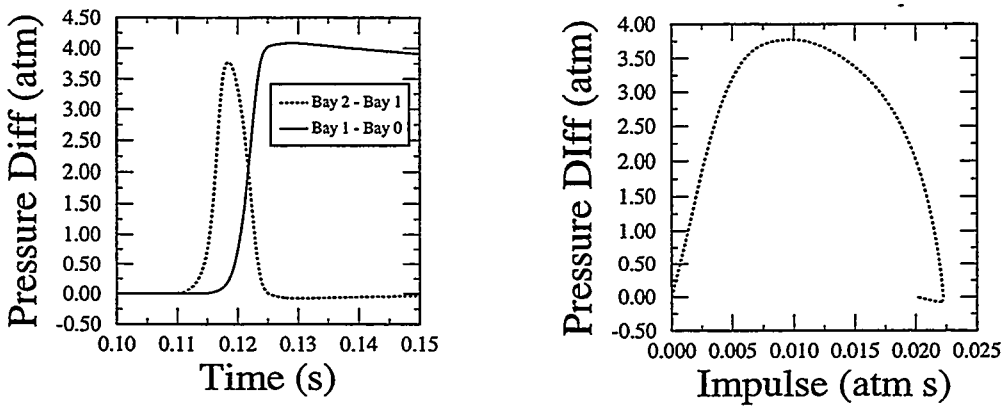

Figure 24. Pressure Differences and Impulse for Ignition Source Location 1.

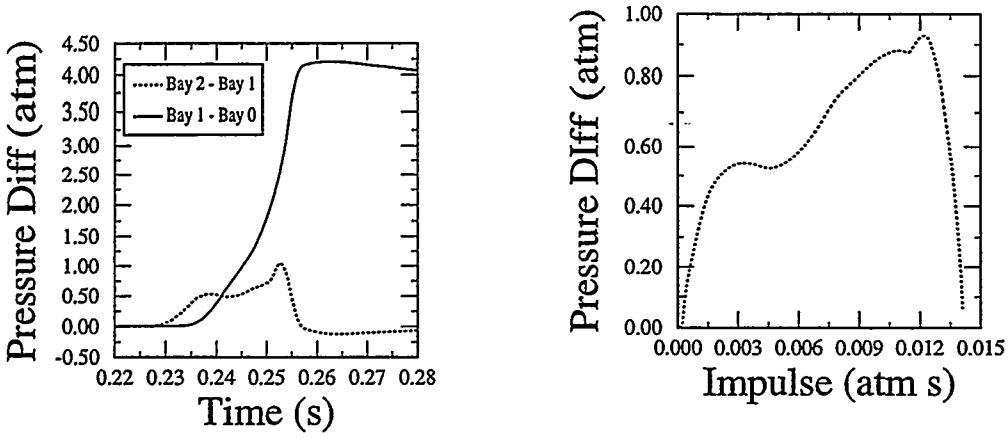

Figure 25. Pressure Differences and Impulse for Ignition Source Location 2

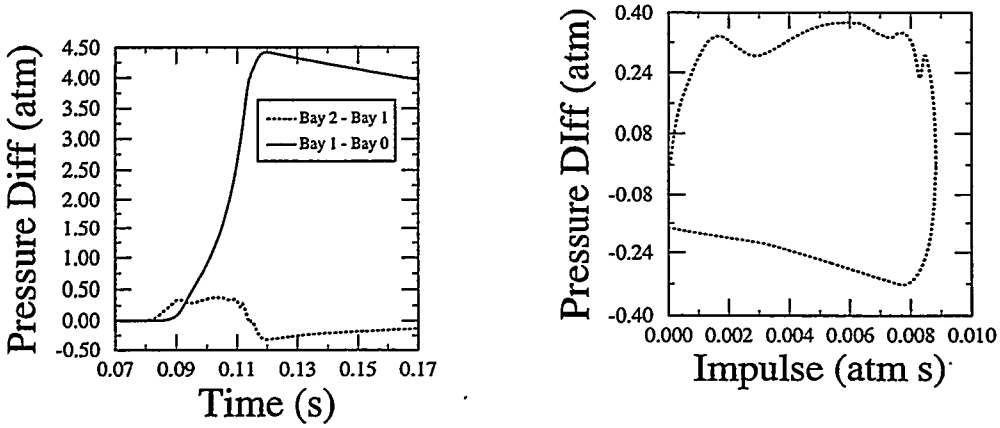

Figure 26. Pressure Differences and Impulse for Ignition Source Location 3

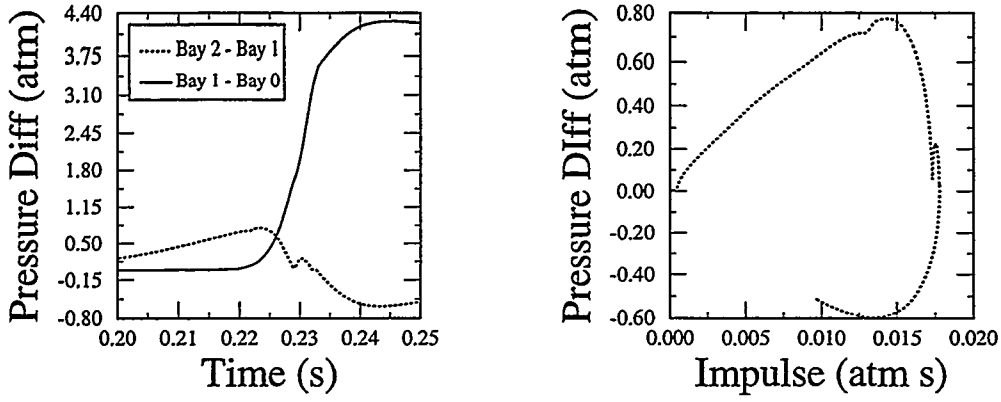

Figure 27. Pressure Differences and Impulse for Ignition Source Location 4

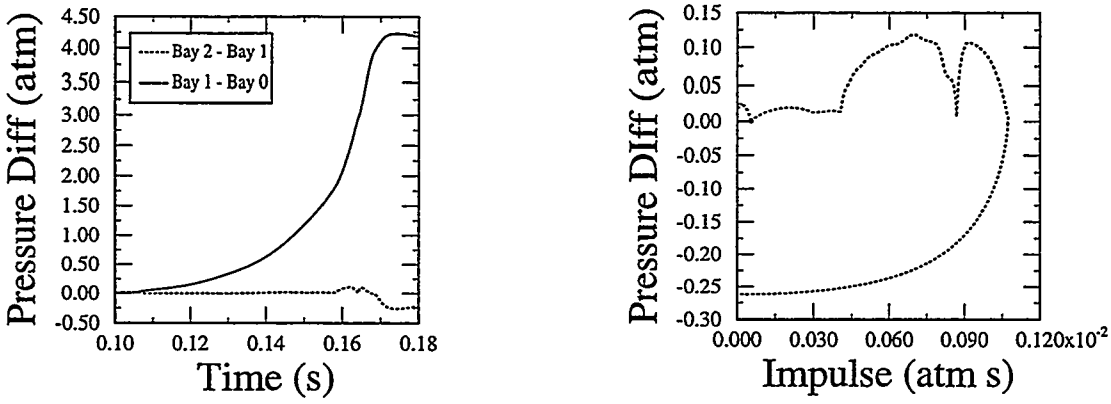

Figure 28. Pressure Differences and Impulse for Ignition Source Location 5

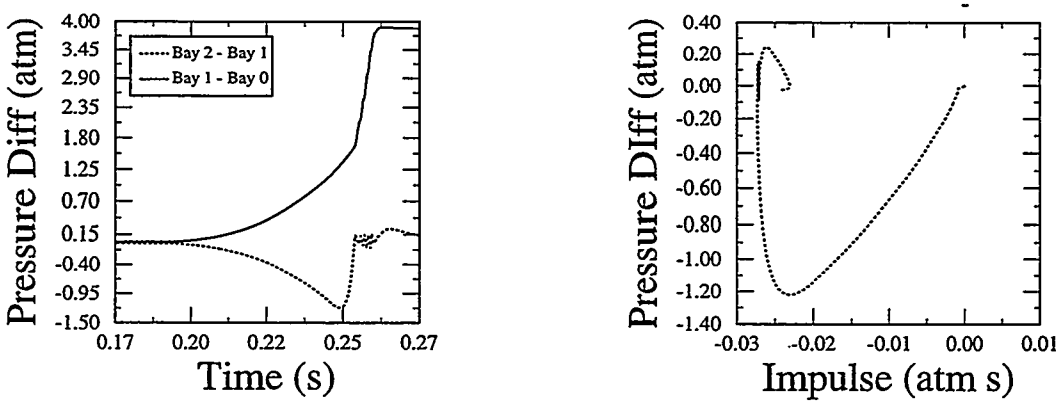

Figure 29. Pressure Differences and Impulse for Ignition Source Location 6

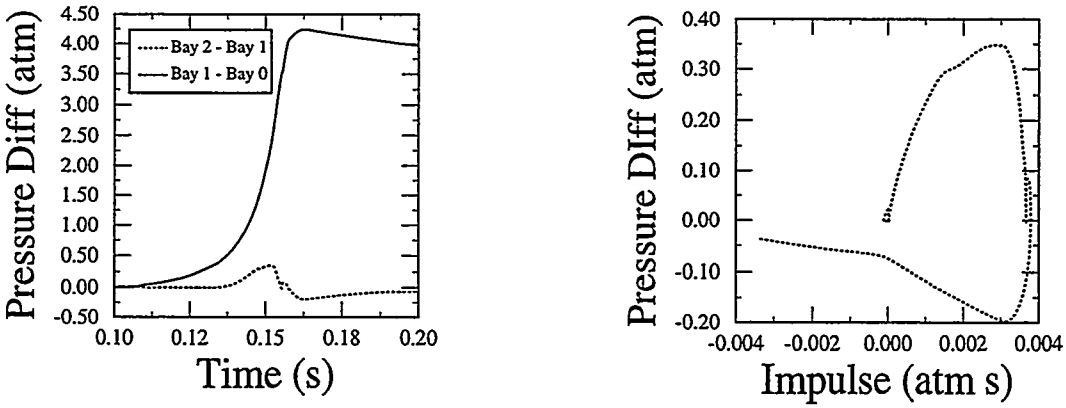

Figure 30. Pressure Differences and Impulse for Ignition Source Location 7

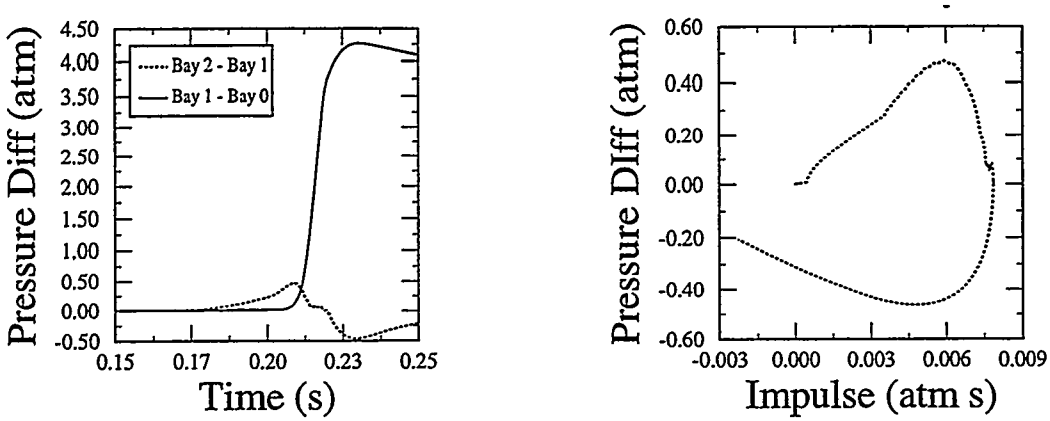

Figure 31. Pressure Differences and Impulse for Ignition Source Location 8

10.0 Conclusions

In support of the NTSB investigation of the TWA 800 accident, a model for three-dimensional flame propagation in multiple enclosures with an arbitrary number of connections between enclosures was developed. This model was then used to support and guide experimental studies to assess the combustion processes which occurred in the center-wing fuel tank of a Boeing 747. The model is computationally efficient because the fluid dynamics has been simplied to neglect acoustic effects (the small Mach number assumption) and detailed flame front resolution is absent (the thin flame assumption). In implementing the flame propagation, a unique, highly efficient three-dimensional adaptive grid refinement technique is used to track multiple burn fronts in multiple connected compartments. Turbulent flame propagation is introduced into the model based on prior studies. Heat transfer effects include thermal radiation and convective heat transfer models. The ability to run cases quikcly and cheaply (workstation compute time is essentially free) contributed greatly to the timliness and success of this study without sacrificing accurate computation of essential quantities such as temperature and pressure. Generalized thermochemical routines for variable fuel-air mixtures are included in this modeling so that additional studies with variable stoichiometry can be made. Currently, this combustion model is decoupled from the mechanical response of the confinement (no structural analysis) and also does not include any multiphase combustion behavior.

Model predictions are compared to one test performed in the CalTech HJET Facility, and in eleven tests conducted in the quarter-scale facility. Overall, the model predictions for pressure histories match well with the measured pressure profiles. These experiments served to provide empirical parameters for the modeling. These parameters were then in turn applied to a study which investigated the liklihood of the eight potential ignition source location in an actual CWT. By examining impulse profiles obtained from computed pressure histories, six of eight ignition locations are doubtful ignition candidates because computed impulse profiles do not match observed impulses on the TWA 800 CWT walls. This approach offers an efficient means for providing appropriate pressure loading conditions for structural failure analysis. Future studies will explore incorporating these routines in dynamic and quasi-static structural failure analysis.

11.0 References

1. National Transportion Safety Board Investigative Hearing on TWA Flight 800, Baltimore, Maryland, December 8-12, 1997.

2. Shepherd, J.E., *et al.*, "Jet A Explosions - Field Test Plan for 1/4 Scale Experiments," California Institute of Technology Report FM97-17, Pasadena, CA, 1997.

3. Brown, L. *et al.*, "Project Status Test Site and Instrumentation/Photoinstrumentation," Presentation by Applied Research Associates, 5941 S. Middlefield Road, Suite 100, Littleton, CO 80123, 1997.

4. Bower, D.R., "Flight Test Group Chairman's Factual Report of Investigation, NTSB Exhibit 23-A, Docket Number SA-516, NTSB Accident Investigation Number DCA96MA070, November 19, 1997.

5. Baer, M.R., and Ratzel, A.C., "A Hydrodynamic Model of Hydrogen Flame Propagation in Reactor Vessels," Proceedings of the Second International Conference on the Impact of Hydrogen on Water Reactor Safety," pp. 757-774, Albuquerque, New Mexico, October, 1982.

6. Sivashinsky, G.T., "Hydrodynamic Theory of Flame Propagation in an Enclosed Volume," Acta Astronautica, Volume 6, pp. 631-645, 1969.

7. Kee, R.J., Rupley, F.M., and Miller, J.A., "The Chemkin Thermodynamic Data Base," Sandia National Laboratories Report SAND87-8215, Sandia National Laboratories, Albuquerque, New Mexico, 87185, April, 1987.

8. Edwards, D.K., "Molecular Gas Band Radiation," Advances in Heat Transfer, Volume 12, T.F. Irvine and J.P. Hartnett, editors, Academic Press, New York, 1976.

9. Shepherd, J.E., *et al.*, "Jet A Explosion Experiments: Laboratory Testing," California Institute of Technology Report FM97-5, Pasadena, CA, 1997.

10. Shepherd, J.E., *et al.*, "Spark Ignition Energy Measurements in Jet-A," California Institute of Technology Report FM97-9, Pasadena, CA, 1997.

11. Barr, P.K., "Acceleration of a Flame by Flame-Vortex Interactions," Combustion and Flame, Volume 82, pp. 111-125, 1990.

12. Abdel-Gayed, R.G. and Bradley, D., "Dependence of Turbulent Burning Velocity on Turbulent Reynolds Number and Ratio of Laminar Burning Velocity to R.M.S. Turbulent Velocity," 16th Symposium (International) on Combustion, pp. 1725-1736, 1967.

13. Lee, J.H.S., and Moen, I.O., "The Mechanism of Transition from Deflagration to Detonation in Vapor Cloud Explosions," Prog. Energy Combustion Science, Volume 6, pp.369-389, 1980.

14. Hinze, J.O., Turbulence, p. 537, Second Edition, McGraw-Hill Publishing, New York, N.Y., 1975.

15. Baker, W.E., *et al.*, Explosion Hazards and Evaluation, Elsevier Scientific Publishing Co., New York, New York, 1983.

Distribution

External Distribution:

Applied Research Associates (4)
5941 S. Middlefield Road, Suite 100
Littleton, CO 80123
Attn: Mr. Peter T. Dzwilewski
Mr. Larry L. Brown
Mr. Robert L. Guice
Mr. Tim Samaras

Dr. Merritt M. Birky
Office of Research and Engineering
National Transportation Safety Board
490 L'Enfant Plaza, S.W.
Washington, D.C. 20594

Dr. Daniel R. Bower
Office of Research and Engineering
National Transportation Safety Board
490 L'Enfant Plaza , S.W.
Washington, D.C. 20594

Mr. Dennis A. Crider
Office of Research and Engineering
National Transportation Safety Board
490 L'Enfant Plaza , S.W.
Washington, D.C. 20594

Dr. Vern Ellingstad
Office of Research and Engineering
National Transportation Safety Board
490 L'Enfant Plaza , S.W.
Washington, D.C. 20594

Dr. Jim Hall
National Transportation Safety Board
490 L'Enfant Plaza , S.W.
Washington, D.C. 20594

Dr. J. Christopher Krok
California Institute of Technology
Mail Stop 205-45
Pasadena, CA 91125

Dr. Julian J. Lee
California Institute of Technology
Mail Stop 301-46
Pasadena, CA 91125

Prof. Joseph E. Shepherd
California Institute of Technology
Mail Stop 105-50
Pasadena, CA 91125

Dr. Paul Thibault
Combustion Dynamics Ltd.
Suite 301, 1888 Brunswick St.
Halifax, Nova Scotia
B3J 3J8

Dr. Kees van Wingerden
Christian Michelson Research AS
Fantoftvegen 38, P.O. Box 3
N-5036 Fantoft, Bergen, Norway

Leo D. Budd
Commander
NAWCWPNS
1 Administration Circle
China Lake, CA 93555-6100

Martin L. Lentz
AFRL/VAVS (WL/FIVS) Bldg 63
1901 Tenth Street
WPAFB, OH 45433-7605

Michael J. Clauson
US Army Tank Automotive and
Armaments Command
Attn: AMSTA-TR-R / 263 (Mr. Clauson)
Warren, MI 48397-5000

Thor Eklund
119 North Drive
Haddonfield, NJ 08033

Thomas L. Wasmund
Code G24
Naval Surface Warfare Center
Dahlgren Division
17320 Dahlgren Road
Dahlgren, VA 22448-5100

Hugh Griffis
NASC/XRA, Bldg 16
2275D Street, Suite10, Room 0067
Wright Patterson AFS, OH 45433-7227

Internal Distribution:

Copy to:

MS 0766	6300	Ellis, D.E.	
MS 0841	9100	Hommert, P.J.	
MS 0828	9101	Bickel, T.C.	
MS 0828	9103	Biffle, J.H.	
MS 0828	9104	Thomas, R.K.	
MS 0826	9111	Hermina, W.	
MS 0824	9112	Ratzel, A.C.	
MS 0824	9112	Baer, M.R.	(10)
MS 0824	9112	Gross, R.J.	(20)
MS 0835	9113	Kempka, S.N.	
MS 0827	9114	Griffith, R.O.	
MS 0825	9115	Rutledge, W.H.	
MS 0836	9116	Peterson, C.W.	
MS 0836	9116	Gritzo, L.A.	
MS 0836	9116	Tieszen, S.R.	
MS 0443	9117	Morgan, H.S.	
MS 9018	8940-2	Central Tech Files	
MS 0899	4916	Technical Library	(2)
MS 0619	12690	Review & Approval Desk For DOE/OSTI	(2)